Quaternary Science Reviews 139 (2016) 77–93

Contents lists available at ScienceDirect

Quaternary Science Reviews

journal homepage: www.elsevier.com/locate/quascirev

Eolian depositional phases during the past 50 ka and inferred climate variability for the Pampean Sand Sea, western Pampas, Argentina

Alfonsina Tripaldi [a, *], Steven L. Forman [b]

[a] IGEBA-CONICET, Dept. of Geological Sciences, University of Buenos Aires, Ciudad Universitaria, Buenos Aires C1428EHA, Argentina
[b] Dept. of Geology, One Bear Place #97354, Baylor University, Waco, TX 76798-7354, USA

ARTICLE INFO

Article history:
Received 5 October 2015
Received in revised form
29 February 2016
Accepted 7 March 2016

Keywords:
Eolian
Pampean Sand Sea
Argentina
Dune field
Paleoclimate

ABSTRACT

The Pampean Sand Sea, which occurs from the Argentinian Pampas to the eastern Andean piedmont, hosts presently stabilized dune fields spanning the late Quaternary. This study integrates previous results and presents new geomorphic, stratigraphic, sedimentological, and chronologic data for nineteen >2 m-thick eolian successions for the San Luis paleo-dune field, western Pampas, to better constrain the depositional history. Six eolian depositional phases are identified spanning the past 50 ka, interposed with paleosols and/or bounded by erosive surfaces. Age control was from 61 OSL ages of small aliquots of quartz grains from eolian stratigraphic units. The inferred timing of eolian phases are at ca. 70 ± 10 yr, 190 ± 20 yr, 12 to 1 ka, 22 to 17 ka, 29 to 24 ka, and 40 to 32 ka. A maximum span for periods of pedogenesis at ca. 12 to 17 ka, 22 to 24 ka, and 29 to 32 ka was provided by bounding OSL ages, which broadly overlap with high stands of pluvial lakes and glacier advances in the central Andes. We infer that the added precipitation may reflect expansion of the Southern Hemisphere monsoon, associated with Northern Hemisphere Heinrich events, leading to episodes of significantly wetter conditions (>350 mm MAP) to at least 35° S. Most of the Holocene (12 ka to 0.8 ka) was characterized by sand sheet deposit under drier than present conditions (100–450 mm MAP), associated with Monte-type vegetation (shrub steppe). The latest two eolian depositional phases, occurred at ca. 190 and 70 yr ago, during the historic period with European settlement and are related to anthropogenic landscape disturbance, though the youngest phase was concomitant with 1930s drought. Wet conditions dominated since ca. AD 1970 with new lakes and rivers forming across this eolian terrain; an incongruous environmental response in reference to drier conditions for most of the Holocene.

1. Introduction

Extensive, late Quaternary deposits of loess and eolian sand occur across central Argentina and are important archives of hydrologic variability, distal to seasonal effects of the South American Monsoon (Clapperton, 1993; Iriondo and Kröhling, 1995; Zárate, 2003, 2007; Rutter et al., 2012; Forman et al., 2014). These presently stabilized eolian landscapes grade texturally from loess and loess-like deposits in the eastern and northern Pampas to sand in the central and western Pampas and the Andean piedmont (Fig. 1). This large eolian sand system, referred to as the "Pampean Sand Sea" (Iriondo, 1990, 1999; Iriondo and Kröhling, 1995), exhibits a diversity of landforms and deposits spanning the past ca. 150 ka (cf. Zárate and Tripaldi, 2012; Tripaldi and Zárate, 2014). The source for these vast eolian deposits are mainly the major west to east flowing rivers emanating from the Andes (Iriondo, 1990), together other sources from the Pampean Ranges and the Brazilian Shield (Morrás, 1999; Zárate, 2003) and possibly contribution of particles by production within the Pampean Sand Sea (cf. Crouvi et al., 2010; Tripaldi et al., 2010). The oldest evidence for activity of the Pampean Sand Sea is an eolian sand deposited beneath the lowermost loess at the Tortugas Site, in southern Santa Fe Province (site 4 in Fig. 1). OSL dating of this lowermost loess yielded a minimum limiting age of ~146 ka and the overlying loess and loessoid deposits that returned OSL ages of ~69 ka and ~63 to 23 ka, within a superimposed, complex paleosol (Kemp et al., 2004). The eastern piedmont of the Pampean ranges, in the northern Pampas (Fig. 1) also show loess, and loessoid successions with intervening paleosols. Particularly, at the OSL dated Lozada site (Córdoba Province; site 3 in Fig. 1), where loess deposition and soil formation

* Corresponding author.
E-mail addresses: alfo@gl.fcen.uba.ar, alfotripaldi@gmail.com (A. Tripaldi).

http://dx.doi.org/10.1016/j.quascirev.2016.03.007
0277-3791/

Fig. 1. Major atmospheric features of the climatic system of South America (ITCZ: Intertropical Convergence Zone, LLJ: Low Level Jet, SACZ: South Atlantic Convergence Zone, Polar advections and Westerlies) and location of the here studied San Luis paleo-dune field and other records mentioned in the text: 1) Tortugas section; 2) Lozada section; 3) Monte Ralo and Corralito sections; 4) Las Lajas section; 5) Baradero section; 6) Hudson and Gorina sections; 7) Médanos de los Naranjos dune field; 8) Médanos Grandes dune field; 9) Médanos Negros dune field; 10) Bebedero lake; 11) Nassau lake; 12) Mar Chiquita lake; 13) Tauca-Coipasa paleolakes. Inset shows with more detail the location of San Luis paleo-dune field. Base images: SRTM3 digital elevation data.

occurred prior to ~80 ka, followed by truncation and deposition of fluvial sediments until ~25 ka, and with renewed loess accumulation until the mid-Holocene (Kemp et al., 2004). Two other sites in this region, Monte Ralo and Corralito (site 2 in Fig. 1) contain three reworked loess deposits separated by paleosols, which yielded OSL ages between 115 and 10 ka (Frechen et al., 2009). Further to the south, in the lowlands of southern Córdoba Province (site 1 in Fig. 1), eolian sand beds were dated to ~18 to 12 ka and ~4 ka (Degiovanni et al., 2005), indicating active deposition during the Late glacial and Holocene.

In central Argentina, the Andean piedmont is covered by extensive dune fields, some with nascent chronologic control which indicates formation and/or reactivation in the latest Pleistocene, and through the Holocene (Tripaldi and Forman, 2007; Zárate and Tripaldi, 2012). The Médanos de los Naranjos dune field (site 7 in Fig. 1) exhibits accretion of an eolian sand sheet and dune movement between ~21 and 14 ka, associated with drier than present conditions (Tripaldi et al., 2011). Médanos Grandes and Médanos Negros dune fields in intermontane valleys confined by the Pampean Ranges and the Andes (sites 8 and 9 in Fig. 1) show younger and repeated reactivations during the Holocene, at ~4.3 to 4, ~2.1 and ~0.6 to 0.4 ka, and at ~2.5 ka, ~0.9 and ~0.5 ka (Fig. 1) (Tripaldi and Forman, 2007). These episodes of dune reactivation are inferred to reflect an intrinsic response to periodic droughts. More recently, in the 1930s the western Pampas experienced a severe drought associated with 30–60% deficit in precipitation (Compagnucci et al., 2002) that was concomitant with agriculture landscape disturbance, which resulted in pervasive reactivation of eolian sand systems (Tripaldi et al., 2013).

The present study focuses on the northern area of the San Luis paleo-dune field in the subtropics of central Argentina (Fig. 1). In the past decade new geomorphic, stratigraphic, and chronologic studies indicated a spatially and a temporally complex eolian depositional system in this area of the western Pampas. These studies have documented pervasive sand sheet deposits near Villa Mercedes in San Luis Province that reflect nearly continuous eolian deposition from ca. 12 ka to 1 ka (Forman et al., 2014). This aggradational eolian system was associated with Monte-type vegetation (shrub steppe) with an inferred mean annual precipitation between 100 and 450 mm and a weakened influence of the South American Monsoon system (SAMS) (Forman et al., 2014). In contrast, the few late Pleistocene records studied, spanning from 40 to 15 ka are characterized by multiple paleosols intercalated with eolian sand reflecting heightened precipitation variability compared to the Holocene (Tripaldi and Forman, 2007; Forman et al., 2014). Previous studies of moraine records for valley glaciers and lake records from the tropical and subtropical Andes inferred significantly wetter, millennial-scale intervals between ca. 60 and 12 ka. These episodes of heightened hydrologic excess are often associated with large melt-water releases into the North Atlantic Ocean from the Laurentide ice sheet, e.g. Heinrich events (Heinrich, 1988), that displaced southward and westward monsoonal sources of precipitation for South America (Markgraf, 1989; Villagrán and Varela, 1990; Sandweiss et al., 1999; Jenny et al., 2002; Abbott et al., 2003; Zech et al., 2009; Placzek et al., 2009; Blard et al., 2011; Tchilinguirian and Morales, 2013). It is unknown if this late Pleistocene precipitation variability penetrated to the western Pampas, near 35° S, and impacted eolian deposition processes.

This contribution presents new geomorphic, stratigraphic, sedimentologic, paleopedologic and chronologic data for >2 m-thick eolian sequences for the San Luis paleo-dune field that span the past 50 ka (Fig. 1). These results, combined with prior observations (Tripaldi and Forman, 2007; Tripaldi et al., 2013; Forman et al., 2014), yield a basis for identifying six eolian depositional phases, formed by successive eolian strata interposed with paleosols and/or bounded by erosive surfaces. Age control was provided by optically stimulated luminescence (OSL) dating of small aliquots of quartz grains from eolian stratigraphic units and this approach has yielded previously a consistent chronology (Tripaldi and Forman, 2007; Tripaldi et al., 2013; Forman et al., 2014). This paper provides new insight into the nature and the timing of eolian depositional phases for the past ca. 50 ka, inferred paleoenvironmental changes; and relation to other late Quaternary records of hydrologic variability in South America and inferred changes in South American Summer Monsoon.

2. Environmental and climatic context

A steep precipitation gradient exists across central Argentina with a mean annual (MAP) precipitation of >1000 mm on the northeastern Pampas to <300 mm MAP to the west across the Andean foothills (cf. Garreaud et al., 2009). There are well-documented ecological regions that parallel this precipitation gradient occurring, from east to west, the Pampean Grassland, the Espinal, and the Monte phytogeographic provinces (cf. Cabrera, 1976; Abraham et al., 2009). The study area is within the Espinal province (~450–600 mm MAP), a savannah-like plain with grasses and scattered trees, which is transitional between the wetter Pampean Grassland to the east (~600–1500 mm MAP) and the drier Monte to the west (~100–450 mm MAP), a shrub steppe with scattered *Prosopis* sp woodlands where groundwater is accessible. A majority of precipitation (>70%) is delivered to western Argentina during the spring and summer (October to March) and reflects influence of the SAMS (Silva and Kousky, 2012). Presently, the San Luis paleo-dune field is a mesic environment with a mean and maximum monthly temperature of 17 °C and 24 °C, respectively, and ~730 mm of annual precipitation (AD 1981–2000; Servicio Meteorológico Nacional). Mean maximum summer temperatures during this rainy season can often exceed 35 °C, enhancing evaporative losses.

The flux of precipitation to western Argentina is associated with the pressure gradient between a thermal-orographic dynamic Chaco Low located east of the Andes and the subtropical South Atlantic Anticyclone (Compagnucci et al., 2002; Doyle and Barros, 2002; Barros et al., 2008). This pressure gradient increases during the austral summer with a maximum in solar insolation, resulting in northeasterly flow and the net import of moisture from the Atlantic Ocean. A significant source of moisture is also derived from the low level meridional Chaco Jet, with maximum wind speeds >15 m s^{-1} at ~1.5 km above ground level, which brings air masses from tropical jungles and humid lowlands of Bolivia and Brazil, southward along the eastern margin of the Andes (Wang and Paegle, 1996; Salio et al., 2002; Marengo et al., 2004) (Fig. 1). The subtropical Andean Cordillera with a mean peak elevation of 4000 m is an effective barrier for the direct import of moisture from the Pacific Ocean, though middle tropospheric Rossby Wave trains associated with strong El Niño events, may enhance convective precipitation in western Argentina with advected sources from the Atlantic Ocean and the western Amazon Basin (Grimm, 2003; Andreoli and Kayano, 2005; Barros et al., 2008; Mendes da Silva and Ambrizzi, 2010).

3. Methods

3.1. Sedimentology and stratigraphy

We present stratigraphic, sedimentologic, and paleopedologic observations for nineteen sections at fifteen sites in the San Luis paleo-dune field (cf. Tripaldi and Forman, 2007; Zárate and Tripaldi, 2012) (Fig. 2). These successions are characterized by depositional units of eolian sand with intercalated paleosols. Usually, eolian stratigraphic successions contain a discontinuous record of depositional periods and associated hiatuses because of the unknown stratigraphic incompleteness associated with eolian erosion and pedogenesis (e.g. Forman et al., 1995; Tripaldi and Forman, 2007; Singhvi and Porat, 2008; Leighton et al., 2014). Thus, we studied multiple sections in this stabilized dune field over five field seasons, in varied geomorphic and stratigraphic contexts, which collectively may reflect the complex history of eolian deposition, landscape

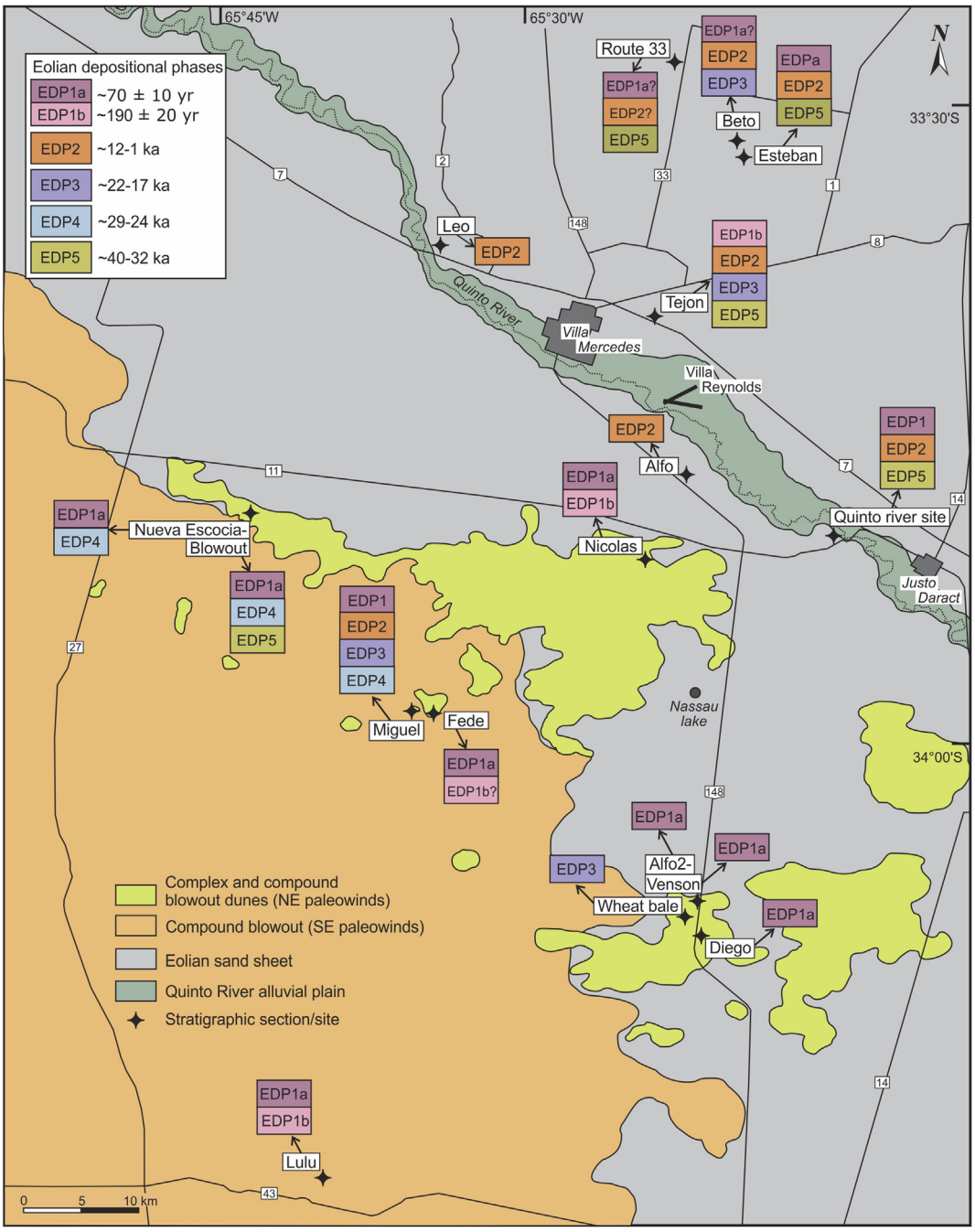

Fig. 2. Geomorphologic map of the San Luis paleo-dune field (western Pampas, Argentina) and locations of the stratigraphic sections showing the eolian depositional phases (EDP).

stability, and inferred paleoenvironmental changes. At several localities tens to hundreds of meters of section are laterally exposed allowing evaluation of the continuity of stratigraphic units. Sections were studied with attention to sedimentologic and pedogenic features. The sedimentology of the exposed deposits were described and interpreted following a well-established facies approach (Reading, 1996). Lithofacies were differentiated in the field based on macroscopic criteria including granulometry, sedimentary structures, and Munsell color, which was assessed in the dry state (Table 1). Also, we recorded changes in bed thickness and the attitude of beds to assess paleowind directions. These measurements are most meaningful where bed dips are >5°. Representative sediments from the identified lithofacies were sampled for granulometry, these samples were pretreated to remove organic matter (with H_2O_2) and carbonates (10% HCl), dispersed into an ultrasonic bath and then measured using a Laser Particle Sizer Malvern 2000. Subsequently, the lithofacies were refined by textural evaluation based on statistical analyses (Folk and Ward, 1957; Boggs, 2006) (Appendix 1). Eolian stratification was interpreted by the criteria of Hunter (1977a, 1977b), Kocurek and Dott (1981) and Lea (1990). Attention was also focused on bedding planes and unit boundaries to assess if there were hiatuses in deposition, indicated by the presence of a buried soil, localized bioturbation or an irregular erosive contact. The recognition and lateral tracing of a buried soil was pivotal because this stratigraphic marker reflects probably landscape stability, associated with

Table 1
Lithofacies of the eolian deposits of San Luis paleo-dune field, western Pampas, Argentina (modified from Miall, 1996). S:L:C indicates the average percentages of sand (S), silt (L) and clay (C).

Lithofacies	Texture	Sedimentary structure	Depositional process	Environmental setting
Sp	Moderately well to well sorted, near symmetrical, fine to very fine sand, with less than 2.5% silt and 0% clay. S:L:C = 99:1:0	Cross-lamination	Eolian dune migration	Dunes
Sh	Moderately to moderately well sorted, near symmetrical to fine skewed, fine to very fine sand, with less than 7.5% of silt and less than 2.6% of clay S:L:C = 96:3:1	Horizontal to very low angle lamination, in some occasion diffuse or partially disrupted, in others associated to isolated ripple-beds	Eolian ripple migration	Eolian sand sheet or mantles associated to blowout dunes
Sm	Moderately to moderately well sorted, symmetrical, fine to very fine sand, with less than 7% of silt and less than 0.2% of clay S:L:C = 96:4:0	Massive	Eolian aggradation by vegetation-disrupted, short-term suspension to modified saltation.	Eolian sand sheet
SLh	Poorly to moderately sorted, near symmetrical to strongly fine skewed, silty sand, with less than 31% of silt and less than 6% of clay S:L:C = 77:20:2	Horizontal to very low angle lamination, in some occasion diffuse or partially disrupted	Eolian ripple migration	Eolian sand sheet
SLm	Poorly to moderately sorted, fine skewed silty sand, with less than 33% of silt and less than 3% of clay S:L:C = 78:21:1	Massive	Eolian aggradation by vegetation-disrupted, short-term suspension to modified saltation.	Eolian sand sheet
LSm	Poorly sorted, near symmetrical to fine skewed, sandy silt. Some beds with few (<5%) of scattered, 1–5 cm pebbles S:L:C = 38:60:7	Massive	Suspension settling	Distal eolian sand sheet or sandy loess plain, partially reworked when pebbly

relatively mesic conditions. We used well-established soil stratigraphic and geomorphic approaches (Birkeland, 1999; Tripaldi and Forman, 2007). Buried soils show clear signs of rubification and secondary accumulation of clay and silt and in places there was evidence for precipitation of pedogenic carbonate (cf. Machette, 1985). Eolian stratigraphic units representing discrete depositional phases were defined by either bounding buried soils or sedimentological characteristics.

3.2. Optically stimulated luminescence dating

Optically stimulating luminescence (OSL) dating used primarily the single aliquot regeneration (SAR) protocols on purified quartz separates (Murray and Wintle, 2003; Wintle and Murray, 2006), similar to previously presented in Forman et al. (2014). Of the 61 OSL ages presented 15 ages are new, with the remaining 47 ages reported previously (Tripaldi and Forman, 2007; Tripaldi et al., 2013; Forman et al., 2014) (Table 2). The multiple aliquot regenerative (MAR) dose method (Jain et al., 2003) was applied to four out of 61 quartz separates (Tripaldi and Forman, 2007). The remaining 57 ages were determined by the SAR protocols on the 63–100, 100–150 or 150–250 μm quartz fraction for 30 to 60 separate aliquots (Table 2; Fig. 3). Quartz extracts dated by MAR and SAR protocols yielded ages that overlap at one sigma errors (Tripaldi and Forman, 2007). Each aliquot contained approximately 100–500 quartz grains corresponding to a 1–2 mm circular diameter of grains adhered (with silicon) to a 1 cm diameter circular aluminum disc. The purity of quartz separates was evaluated by petrographic inspection and point counting of a representative aliquot. Samples that showed >1% of non-quartz minerals were retreated with HF and rechecked petrographically. The spectral purity of quartz separates was tested by exposing aliquots to infrared excitation (1.08 W from a laser diode at 845 ± 4 nm), which preferentially excites feldspar minerals. Samples measured showed weak emissions (<200 counts/second), at or close to background counts with infrared excitation, and ratio of emissions from blue to infrared excitation of >20, indicating a spectrally pure quartz extract (Duller, 2003). The majority of aliquots (>90%) exhibited a clear, so-called fast component, with a "fast ratio" of >10 (cf. Durcan and Duller, 2011) which is one of the requirements of the SAR dating protocols (Murray and Wintle, 2003).

Calculation of equivalent dose by the single aliquot protocols was accomplished for 21 to 50 aliquots (Table 2). Aliquots were removed from analysis because the recycling ratio was not between 0.90 and 1.10, the zero dose was >5% of the natural emissions, or the error in D_e determination is >10%. Equivalent dose (D_e) distributions for most samples were log normal and exhibited overdispersion values ≤20% (at two-sigma errors), except for the youngest samples, ca. ≤200 years old (Table 2; Fig. 3). An overdispersion percentage of a D_e distribution is an estimate of the relative standard deviation from a central D_e value in context of a statistical estimate of errors (Galbraith et al., 1999; Galbraith and Roberts, 2012). A zero overdispersion percentage indicates high internal consistency in D_e values with 95% of the D_e values within 2σ errors. Overdispersion values ≤20% are routinely assessed for small aliquots of quartz grains that are well solar reset, like eolian sands (e.g., Olley et al., 1998; Wright et al., 2011 Meier et al., 2013) and this value is considered a conservative threshold metric for calculation of a D_e value using the central age model (CAM) of Galbraith et al. (1999). We consider overdispersion values >20% (at one sigma limits) to indicate post depositional mixing of grains, grains of various ages, partial solar resetting of grains or complex microdosimetry; the Finite Mixture Model (FMM) is an appropriate statistical treatment for such data (Galbraith and Green, 1990), and this model was used for quartz extracts that yielded overdispersion values of ≥25% (Table 2).

A determination of the environmental dose rate is needed to render an optical age, which is an estimate of the exposure of quartz grains to ionizing radiation from U and Th decay series, ^{40}K, and cosmic sources during the burial period (Table 2). The U and Th content of the sediments, assuming secular equilibrium in the decay series and ^{40}K, were determined by inductively coupled plasma-mass spectrometry (ICP-MS/OES) analyzed by Activation Laboratory LTD, Ontario, Canada. The beta and gamma doses were adjusted according to grain diameter to compensate for mass attenuation (Fain et al., 1999). A significant cosmic ray component

Table 2
Optically stimulated luminescence (OSL) age on quartz grains from eolian deposits San Luis paleo-dune field, western Pampas, Argentina.

Sample	Laboratory number	Aliquots	Grain size (microns)	Equivalent dose (Gray)[a]	Over-dispersion (%)[b]	U (ppm)[c]	Th (ppm)[c]	K %)[c]	H_20 (%)	Cosmic dose (mGray/yr)[d]	Dose rate (mGray/yr)	OSL age (yr)[e]	Reference
Eolian Depositional Phase 1a: 14 OSL ages at 15 sites (70 ± 10 yr)													
SL05-23	UIC1610Bl	30/30	63–100	0.26 ± 0.01	35 ± 5	2.5 ± 0.1	9.4 ± 0.1	2.88 ± 0.03	5 ± 2	0.12 ± 0.01	4.04 ± 0.17	65 ± 5	Tripaldi and Forman, 2007
SL05-27	UIC1714Bl	29/30	63–100	0.35 ± 0.05	40 ± 4	2.3 ± 0.1	7.9 ± 0.1	2.66 ± 0.03	5 ± 2	0.17 ± 0.02	3.67 ± 0.16	95 ± 10	Tripaldi and Forman, 2007
SL05-28	UIC1611Bl	30/30	63–100	0.26 ± 0.03	54 ± 5	2.2 ± 0.1	8.2 ± 0.1	2.78 ± 0.03	5 ± 2	0.18 ± 0.02	3.95 ± 0.17	70 ± 10	Tripaldi and Forman, 2007
SL05-29	UIC1715	28/30	63–100	0.33 ± 0.01	34 ± 4	2.2 ± 0.1	7.6 ± 0.1	2.70 ± 0.03	5 ± 2	0.16 ± 0.02	3.78 ± 0.17	90 ± 10	Tripaldi and Forman, 2007
SL05-32	UIC1609	28/30	63–100	0.06 ± 0.01	83 ± 10	2.1 ± 0.1	7.5 ± 0.1	2.60 ± 0.03	5 ± 2	0.18 ± 0.02	3.78 ± 0.17	15 ± 2	Tripaldi and Forman, 2007
SL08-16	UIC2376	50/50	63–100	0.32 ± 0.01	76 ± 9	2.0 ± 0.1	7.1 ± 0.1	2.18 ± 0.02	10 ± 3	0.16 ± 0.02	3.32 ± 0.16	70 ± 10	Tripaldi and Forman, 2007
SL10-20	UIC3272	31/45	63–100	0.22 ± 0.02	45 ± 5	2.2 ± 0.1	7.5 ± 0.1	2.06 ± 0.02	5 ± 2	0.20 ± 0.02	3.22 ± 0. 16	60 ± 5	Forman et al., 2014
SL10-30	UIC2805	25/30	63–100	0.23 ± 0.01	50 ± 6	2.0 ± 0.1	7.4 ± 0.1	2.30 ± 0.02	5 ± 2	0.21 ± 0.02	3.02 ± 0.15	70 ± 10	Forman et al., 2014
SL10-42	UIC3284	29/30	100–150	0.20 ± 0.01	42 ± 5	2.0 ± 0.1	7.0 ± 0.1	2.07 ± 0.02	10 ± 3	0.13 ± 0.01	2.81 ± 0.14	60 ± 10	Forman et al., 2014
SL10-44	UIC3286	44/50	100–150	0.26 ± 0.01	73 ± 8	2.1 ± 0.1	7.0 ± 0.1	2.16 ± 0.02	5 ± 2	0.14 ± 0.01	3.08 ± 0.15	75 ± 10	Forman et al., 2014
SL10-45	UIC3281	27/30	100–150	0.26 ± 0.02	90 ± 14	2.2 ± 0.1	7.4 ± 0.1	2.18 ± 0.02	5 ± 2	0.16 ± 0.02	3.16 ± 0.16	70 ± 10	Forman et al., 2014
VM12-24	BG3596	27/30	63–100	0.37 ± 0.03	96 ± 13	1.7 ± 0.1	5.6 ± 0.1	1.93 ± 0.02	5 ± 2	0.19 ± 0.02	2.67 ± 0.14	80 ± 10	This paper
VM12-25	BG3838	28/30	100–150	0.21 ± 0.02	86 ± 12	2.1 ± 0.1	6.6 ± 0.1	2.11 ± 0.02	5 ± 2	0.18 ± 0.02	3.04 ± 0.16	60 ± 10	This paper
VM12-26	BG3839	32/48	100–150	0.24 ± 0.02	113 ± 15	2.3 ± 0.1	6.9 ± 0.1	2.14 ± 0.02	5 ± 2	0.15 ± 0.02	3.12 ± 0.16	70 ± 10	This paper
											mean & SD	72 ± 7[f]	
Eolian Depositional Phase 1b: 3 OSL ages at 3 sites (190 ± 20 yr)													
SL10-12	UIC2801	27/30	63–100	0.68 ± 0.03	42 ± 6	3.1 ± 0.1	8.4 ± 0.1	2.16 ± 0.03	5 ± 2	0.18 ± 0.02	3.57 ± 0.18	180 ± 15	Forman et al., 2014
SL08-18	UIC2377	30/30	63–100	0.63 ± 0.06	42 ± 5	2.1 ± 0.1	7.5 ± 0.1	2.17 ± 0.03	10 ± 3	0.15 ± 0.02	3.15 ± 0.16	200 ± 20	Forman et al., 2014
VM12-22	BG3595	27/30	63–100	0.68 ± 0.03	42 ± 6	3.1 ± 0.1	8.4 ± 0.1	2.16 ± 0.03	5 ± 2	0.18 ± 0.02	3.57 ± 0.18	180 ± 15	This paper
											mean & SD	190 ± 20	
Eolian Depositional Phase 2: 28 OSL ages at 10 sites (ca. 12–1 ka)													
SL08-04	UIC2371	30/30	63–100	14.46 ± 0.63	16 ± 2	2.4 ± 0.1	8.8 ± 0.1	2.22 ± 0.02	5 ± 2	0.18 ± 0.02	3.48 ± 0.23	4135 ± 300	Forman et al., 2014
SL08-06	UIC2372	30/30	63–100	15.49 ± 0.71	18 ± 2	2.4 ± 0.1	8.8 ± 0.1	2.19 ± 0.02	5 ± 2	0.17 ± 0.02	3.45 ± 0.22	4480 ± 330	Forman et al., 2014
SL08-08	UIC2373	30/30	63–100	21.24 ± 1.04	19 ± 2	2.5 ± 0.1	9.3 ± 0.1	2.21 ± 0.02	10 ± 3	0.16 ± 0.02	3.33 ± 0.21	6365 ± 505	Forman et al., 2014
SL08-11	UIC2375	30/30	63–100	16.27 ± 0.81	19 ± 2	2.3 ± 0.1	8.2 ± 0.1	2.10 ± 0.02	5 ± 2	0.18 ± 0.02	3.31 ± 0.22	4910 ± 380	Forman et al., 2014
SL08-13	UIC2499	33/35	63–100	38.12 ± 1.86	20 ± 3	3.0 ± 0.1	9.8 ± 0.1	2.12 ± 0.02	10 ± 3	0.16 ± 0.02	3.39 ± 0.22	11,210 ± 870	Forman et al., 2014
SL08-19	UIC2501	33/35	63–100	4.01 ± 0.15	22 ± 3	2.6 ± 0.1	9.0 ± 0.1	2.33 ± 0.02	2 ± 1	0.17 ± 0.02	3.77 ± 0.26	1070 ± 70	Forman et al., 2014
SL08-20	UIC2729	26/30	100–150	8.46 ± 0.23	20 ± 3	2.5 ± 0.1	8.9 ± 0.1	2.19 ± 0.02	5 ± 2	0.16 ± 0.02	3.35 ± 0.22	2515 ± 150	Forman et al., 2014
SL08-21	UIC2578	29/30	63–100	17.45 ± 0.78	17 ± 2	2.5 ± 0.1	8.8 ± 0.1	2.26 ± 0.02	5 ± 2	0.14 ± 0.01	3.51 ± 0.23	4960 ± 385	Forman et al., 2014
SL08-22	UIC2730	28/30	100–150	21.02 ± 1.06	19 ± 2	2.6 ± 0.1	9.1 ± 0.1	2.22 ± 0.03	5 ± 2	0.13 ± 0.01	3.39 ± 0.22	6185 ± 475	Forman et al., 2014
SL08-24	UIC2577	30/30	100–150	25.49 ± 1.10	14 ± 1	2.1 ± 0.1	7.5 ± 0.1	2.06 ± 0.02	5 ± 2	0.11 ± 0.01	3.00 ± 0.16	8490 ± 620	Forman et al., 2014
SL08-27	UIC2502	32/35	63–100	41.15 ± 1.98	16 ± 2	2.8 ± 0.1	9.3 ± 0.1	2.03 ± 0.02	10 ± 3	0.09 ± 0.01	3.36 ± 0.22	12,260 ± 910	Forman et al., 2014
SL08-35	UIC2344	28/30	63–100	5.61 ± 0.31	23 ± 3	1.9 ± 0.1	6.7 ± 0.1	2.15 ± 0.02	2 ± 1	0.21 ± 0.02	3.24 ± 0.21	1720 ± 140	Forman et al., 2014
SL08-36	UIC2731	30/30	100–150	25.49 ± 1.10	12 ± 2	2.1 ± 0.1	7.5 ± 0.1	2.06 ± 0.02	5 ± 2	0.11 ± 0.01	3.00 ± 0.16	8490 ± 620	Forman et al., 2014
SL08-37	UIC2346	29/30	63–100	33.78 ± 1.72	20 ± 3	2.0 ± 0.1	7.3 ± 0.1	2.09 ± 0.02	10 ± 3	0.14 ± 0.01	2.95 ± 0.15	11,455 ± 940	Forman et al., 2014
SL10-01	UIC3278	27/30	100–150	15.99 ± 0.84	21 ± 3	2.1 ± 0.1	7.2 ± 0.1	2.12 ± 0.02	2 ± 1	0.14 ± 0.01	3.15 ± 0.16	5215 ± 415	Forman et al., 2014
SL10-02	UIC3280	31/40	100–150	2.44 ± 0.13	22 ± 3	2.1 ± 0.1	7.1 ± 0.1	2.07 ± 0.02	5 ± 2	0.19 ± 0.02	3.05 ± 0.16	790 ± 60	Forman et al., 2014
SL10-04	UIC3271	27/30	100–150	10.31 ± 0.49	18 ± 2	2.0 ± 0.1	6.8 ± 0.1	2.12 ± 0.02	5 ± 2	0.17 ± 0.02	3.14 ± 0.16	3265 ± 240	Forman et al., 2014
SL10-09	UIC2804	29/30	63–100	29.52 ± 1.47	19 ± 2	3.0 ± 0.1	8.4 ± 0.1	2.10 ± 0.03	5 ± 2	0.15 ± 0.01	3.46 ± 0.18	8510 ± 645	Forman et al., 2014
SL10-11	UIC2806	30/35	63–100	5.09 ± 0.25	21 ± 3	2.5 ± 0.1	8.8 ± 0.1	2.21 ± 0.03	5 ± 2	0.17 ± 0.01	3.50 ± 0.18	1440 ± 110	Forman et al., 2014
SL10-13	UIC3276	28/30	100–150	32.73 ± 1.69	20 ± 3	2.5 ± 0.1	8.5 ± 0.1	2.20 ± 0.02	10 ± 3	0.13 ± 0.01	3.13 ± 0.16	10,440 ± 850	Forman et al., 2014
SL10-15	UIC3478	27/30	63–100	19.26 ± 1.10	24 ± 4	2.8 ± 0.1	9.1 ± 0.1	2.12 ± 0.02	5 ± 2	0.17 ± 0.02	3.50 ± 0.18	5490 ± 440	Forman et al., 2014
SL10-24	UIC3273	37/40	150–250	31.94 ± 1.61	23 ± 3	2.6 ± 0.1	8.5 ± 0.1	2.20 ± 0.02	10 ± 3	0.12 ± 0.01	3.09 ± 0.16	10,315 ± 830	Forman et al., 2014
SL10-26	UIC3479	28/30	63–100	33.75 ± 1.94	24 ± 3	2.6 ± 0.1	9.1 ± 0.1	2.13 ± 0.02	5 ± 2	0.15 ± 0.02	3.44 ± 0.17	9785 ± 795	Forman et al., 2014
SL10-28	UIC2802	25/30	63–100	6.66 ± 0.30	22 ± 3	2.7 ± 0.1	8.4 ± 0.1	2.16 ± 0.03	5 ± 2	0.18 ± 0.02	3.48 ± 0.18	1905 ± 140	Forman et al., 2014
VM12-03	BG3594	34/48	63–100	11.69 ± 0.54	19 ± 2	2.4 ± 0.1	8.0 ± 0.1	2.07 ± 0.03	5 ± 2	0.17 ± 0.02	3.28 ± 0.17	3550 ± 260	This paper
VM12-05	BG3597	28/30	63–100	37.53 ± 1.85	19 ± 3	2.5 ± 0.1	7.9 ± 0.1	2.07 ± 0.02	5 ± 2	0.14 ± 0.01	3.26 ± 0.17	11,480 ± 875	This paper
VM12-06	BG3991	31/35	100–150	36.56 ± 1.75	19 ± 2	2.6 ± 0.1	9.0 ± 0.1	2.11 ± 0.02	10 ± 3	0.12 ± 0.01	3.10 ± 0.16	11,790 ± 920	This paper
Eolian Depositional Phase 3: 6 OSL ages at five sites (ca. 17–22 ka)													
SL08-29	UIC2503	28/30	100–150	62.87 ± 3.08	19 ± 3	2.5 ± 0.1	8.8 ± 0.1	2.09 ± 0.02	5 ± 2	0.17 ± 0.02	3.21 ± 0.21	19,580 ± 1505	This paper
SL08-39	UIC2345	30/30	63–100	63.58 ± 2.66	12 ± 2	2.3 ± 0.1	10.1 ± 0.1	2.23 ± 0.02	5 ± 2	0.11 ± 0.01	3.51 ± 0.23	18,130 ± 1300	Forman et al., 2014
SL10-03	UIC2803	29/30	63–100	56.49 ± 1.85	18 ± 2	2.9 ± 0.1	9.0 ± 0.1	1.99 ± 0.02	10 ± 3	0.13 ± 0.01	3.18 ± 0.16	17,140 ± 1110	Forman et al., 2014
SL10-08	UIC3279	29/30	100–150	67.45 ± 4.55	21 ± 3	2.4 ± 0.1	7.6 ± 0.1	2.13 ± 0.02	5 ± 2	0.16 ± 0.02	3.16 ± 0.16	21,315 ± 1900	Forman et al., 2014
VM12-07	BG3598	39/48	63–100	69.69 ± 3.65	22 ± 3	2.7 ± 0.1	8.0 ± 0.1	2.09 ± 0.02	10 ± 3	0.15 ± 0.02	3.17 ± 0.16	21,980 ± 1780	This paper

VM12-09	BG3992	30/40	100–150	64.87 ± 3.43	22 ± 3	2.7 ± 0.1	8.8 ± 0.1	2.12 ± 0.02	10 ± 3	0.17 ± 0.02	3.16 ± 0.16 mean & SD	20,530 ± 1650 19,670 ± 2190	This paper
Eolian Depositional Phase 4: 5 OSL ages at three sites (ca. 24–29 ka)													
SL05-19	UIC1608GR	MAR	150–250	96.36 ± 3.29		2.3 ± 0.1	9.4 ± 0.1	2.74 ± 0.03	5 ± 2	0.13 ± 0.01	3.54 ± 0.16	27,185 ± 2280	Tripaldi and Forman, 2007
SL05-22	UIC1613GR	MAR	150–250	90.59 ± 0.19		2.1 ± 0.1	7.9 ± 0.1	2.57 ± 0.03	5 ± 2	0.15 ± 0.02	3.67 ± 0.16	24,700 ± 1500	Tripaldi and Forman, 2007
SL05-26	UIC1607GR	MAR	150–250	107.23 ± 4.07		2.5 ± 0.1	9.0 ± 0.1	2.87 ± 0.03	5 ± 2	0.14 ± 0.01	3.88 ± 0.17	27,650 ± 2085	Tripaldi and Forman, 2007
SL05-26	UIC1607BI	28/30	150–250	91.19 ± 3.87	19 ± 3	2.5 ± 0.1	9.0 ± 0.1	2.87 ± 0.03	5 ± 2	0.14 ± 0.01	3.88 ± 0.17	23,500 ± 1830	Tripaldi and Forman, 2007
SL08-41	UIC2347	38/40	63–100	90.39 ± 4.21	16 ± 2	2.2 ± 0.1	8.0 ± 0.1	2.18 ± 0.02	10 ± 3	0.10 ± 0.01	3.19 ± 0.17 mean & SD	27,700 ± 2100 26,120 ± 2610	This paper
Eolian Depositional Phase 5: 5 OSL ages at five sites (ca. 40–32 ka)													
SL05-25	UIC1616Gr	MAR	150–250	122.97 ± 1.06		2.4 ± 0.1	8.9 ± 0.1	2.79 ± 0.03	10 ± 3	0.12 ± 0.01	3.76 ± 0.16	32,700 ± 2150	Tripaldi and Forman, 2007
SL08-10	UIC2374	30/30	100–150	138.00 ± 10.86	15 ± 2	4.6 ± 0.1	9.4 ± 0.1	2.85 ± 0.03	10 ± 3	0.12 ± 0.01	4.20 ± 0.21	32,675 ± 2890	This paper
SL10-23	UIC3292	31/40	63–100	131.03 ± 9.29	21 ± 3	2.9 ± 0.1	8.6 ± 0.1	2.25 ± 0.02	10 ± 3	0.12 ± 0.01	3.37 ± 0.17	38,535 ± 3380	This paper
SL10-38	UIC3283	21/30	100–150	121.37 ± 6.36	18 ± 3	2.3 ± 0.1	7.7 ± 0.1	2.18 ± 0.02	5 ± 2	0.12 ± 0.01	3.18 ± 0.16	38,190 ± 3020	This paper
VM12-10	BG3820	46/60	63–100	114.38 ± 8.41	48 ± 4	2.5 ± 0.1	8.8 ± 0.1	2.19 ± 0.02	15 ± 5	0.17 ± 0.01	3.33 ± 0.17 mean & SD	34,330 ± 3540 35,260 ± 3670	This paper
Unnamed Eolian Depositional Phase													
SL10-33	UIC3287	25/35	100–150	160.95 ± 10.54	23 ± 3	3.6 ± 0.1	8.2 ± 0.1	1.98 ± 0.02	10 ± 3	0.12 ± 0.01	3.16 ± 0.16	51,010 ± 4525	This paper

[a] Equivalent dose (D_e) analyzed under blue-light excitation (470 ± 20 nm) by single aliquot regeneration protocols (Murray and Wintle, 2003; Wintle and Murray, 2006), except for SL05-19, SL05-22, and SL05-26 with the D_e determined by multiple aliquot regenerative (MAR) dose method (Jain et al., 2003).

[b] Values reflect precision beyond instrumental errors; values of ≤20% (at 2 sigma errors) indicate low dispersion in equivalent dose values with a log-normal unimodal distribution. Overdispersion values of >30% indicates dispersion beyond a single log normal distribution, with possible mixture of grains of various ages; for these analysis the minimum age model was used to calculate the equivalent dose (cf. Galbraith and Roberts, 2012).

[c] U, Th and K_20 content analyzed by inductively coupled plasma-mass spectrometry analyzed by Activation Laboratory LTD, Ontario, Canada.

[d] From Prescott and Hutton (1994).

[e] Systematic and random errors calculated in a quadrature at one standard deviation. Datum year is AD 2000.

[f] Average and standard deviation calculated using all values except SL05-32.

between 0.10 and 0.21 mGy/yr was included in the estimated dose rate taking into account the current depth of burial (Prescott and Hutton, 1994). A moisture content (by weight) of 5 ± 2%, 10 ± 3, or 15 ± 5% was used in dose rate calculations, which reflects the variability in current field moisture conditions. The datum year for all OSL ages is AD 2000 to be compatible with previous reported ages (cf. Tripaldi and Forman, 2007; Tripaldi et al., 2013; Forman et al., 2014).

4. Results

4.1. Geomorphology and stratigraphy

The studied eolian system has two geomorphic domains: a northern area dominated by a sand sheet and a paleo-dune field to the south with a variety of dune morphologies (Fig. 2). The sand sheet area constitutes a mostly flat or low relief surface composed of fine sand to silty sand. Locally, there are some linear streaks (cf. McKee, 1979: 10) recognized from Landsat TM images and SRTM digital elevation data, having a low topographic expression (<1 m) in the field. The Quinto River has incised into the sand sheet and this river is close to the transitional boundary between the proximal sand sheet to the south and the distal sand sheet over upland surfaces, north of the river (Fig. 2). The proximal sand sheet, adjacent to a dune area, is dominated by moderately to well sorted, fine sand and <4% silt, whereas the distal facies is composed of poorly sorted, fine to very fine sand with 4–20% silt (cf. Forman et al., 2014).

The most characteristic eolian landform of the dune area is a series of crater-like depressions, with sub-rounded to elliptic forms and diameters of tens to hundreds of meters, classified as blowout dunes (Tripaldi and Forman, 2007). Several of the blowout dunes for this paleo-dune field present a leeside depositional lobe covered by smaller dunes (blowouts/barchanoid ridges) and thus, are compound/complex dunes (cf. McKee, 1979). These blowout dunes vary in size between 300 and 3500 m in diameter, with depositional lobes rising between 5 and 20 m above the adjacent plain. The dunes show two main orientations. One group of blowout dunes have depositional lobes orientated to the NW (mean azimuth 125°), indicating formation by southeasterly paleowinds, whereas in the northeasterly area the depositional lobes are located to the SW (mean azimuth 69°), indicating paleowinds from the northeast. Perennial lakes occur commonly in the blowout dunes.

The sedimentary cover of the study area is dominated by several meter-thick, fine sand to silty sand of eolian origin. Fluvial deposits are confined mostly between the channel of the Quinto River and the highest recognized terrace at 8–10 m above the present channel. To the north, the eolian cover loam is associated with fluvial deposits related to the recently formed “new rivers” (Contreras et al., 2013) and from older streams that drained the ranges (Fig. 1). Here we present solely results for the eolian depositional record, which is well expressed in this area.

Nineteen stratigraphic sections were studied in the San Luis paleo-dune field which exposed sequences of eolian sediment up to 9-m thick, with six eolian lithofacies recognized by particle size and sedimentary structures (Table 1). These deposits, as indicated by OSL ages, span from ~50 ka ago to the 20th century (Table 2). The integration of previously presented sections (Tripaldi and Forman, 2007; Tripaldi et al., 2013; Forman et al., 2014), and new observations for the oldest dated stratigraphic units, provides a larger data base for inferring the extent, timing and paleoenvironmental significance of the eolian deposits in the western Pampas.

The eolian deposits cluster texturally into two broad groups,

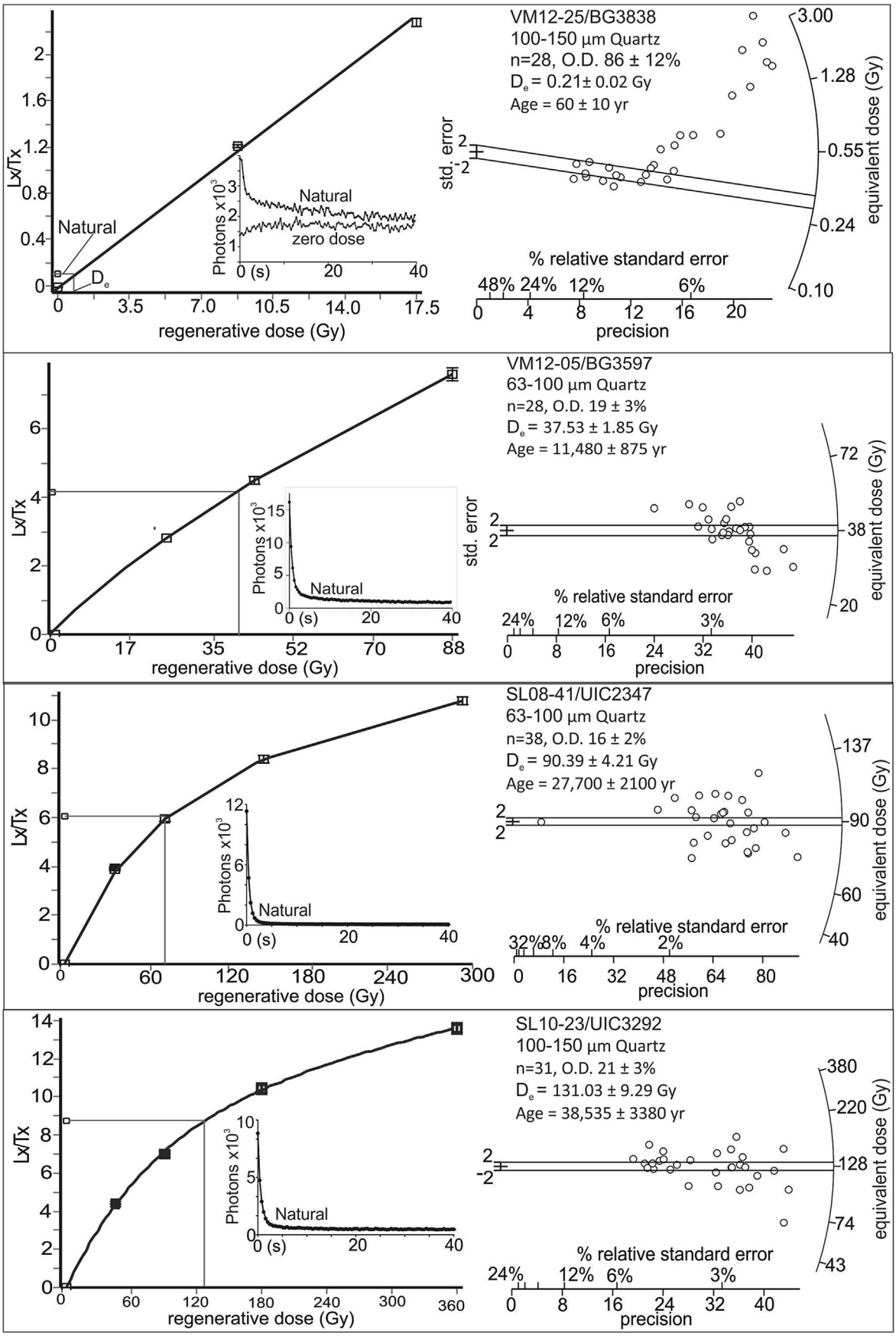

Fig. 3. Single aliquot regenerative (SAR) dose response curve, with inset figure showing representative shine down curve, and adjacent figure a radial plot of equivalent dose values for samples for four representative quartz extracts.

which is consistent with the two recognized geomorphologic domains. The southern dune area is dominated by moderately well sorted, symmetrical, fine sand, with <7.5% of silt and without or only traces of clay (mean values of sand, silt and clay of 76.10%, 21.95% and 0.39%, respectively, Fig. 4, Appendix 1). In contrast, the northern sand sheet deposits are composed of moderately sorted, positive skewed, silty sand, with ~76.10% of sand, a higher and a variable percentage of silt (~14%–~33%), and small quantities of clay (~1.95%) (Fig. 4, Appendix 1). In two localities, at Esteban, Route 33 and Road cut A sections, there are basal beds with higher percentage of silt (40–60%) but still low amounts of clay (<7%), corresponding to a poorly sorted, positive skewed, sandy silt (Fig. 4).

The most common eolian deposits are a fine sand (Sh lithofacies) and a silty sand (SLh lithofacies), characterized by millimeter-to-centimeter-scale, horizontal to very low-angle laminations (<10°), often with inverse grading within individual lamina (Table 1). In some sections these sediments are associated with isolated ripple-formed lamina. All these features are consistent with deposition by eolian ripple migration (Hunter, 1977a, 1977b), in a sand sheet environment or mantles associated with blowout dunes. In some beds the Sh and SLh lithofacies appear diffuse or partially disrupted, that may reflect syn-deposition with grasses and small-scale bioturbation, probably from insects.

Other widespread deposits are massive, fine sand (Sm lithofacies) and silty sand (SLm lithofacies) (Table 1). In various sections 1- to 4-cm long bed remnants are commonly interlayered with numerous centimeter- to decimeter-wide trace sub-fossils, indicating extensive burrowing. Similar massive beds also occur below paleosols, reflecting pedoturbation. In contrast, there are up to 3-m thick, massive sands in some stratigraphic exposures which may be primarily depositional, with no evidence of pedogenesis and little indication of burrowing. In eolian sand sheets, sediment deposition is also associated with unrippled, flat or undulatory surfaces (cf. Pye and Tsoar, 2009) where a massive bed reflects grain transportation by short-term suspension and modified saltation, which inhibit the formation of ripples (cf. Lea, 1990). This eolian sedimentation was associated with a sparsely vegetated land surface (cf. Lea, 1990) and in distal zones of sand sheets (cf. Forman et al., 2014).

Less common deposits are beds of massive, sandy silt, with low clay content and absence of sediments coarser than a medium sand (LSm lithofacies, Table 1), that reflect a dominance of eolian suspension settling and thus, was interpreted as a distal sand sheet or a sandy loess-like deposit (Ruegg, 1983; Pye and Tsoar, 2009: 153). In places these deposits exhibit lenses with few (<5%) scattered, 1–5 cm diameter pebbles, suggesting partial alluvial reworking by local runoff.

Various sections show units with cross-bedding (Sp lithofacies), which are composed of fine to very fine, very well sorted sand, with a low content of silt and generally without clay (Table 1). Bed thickness was centimeter-scale to up to 1 m thick, forming up to 6 m-thick successions. Bed inclinations varied between 15° and 30°, and beds with dips of >25° which were often asymptotic reflecting avalanche processes. This facies appears related to complex blowout dunes on the surface associated with 19th to early 20st century landscape disturbances (cf. Tripaldi et al., 2013). The textural and bedding characteristics of these deposits were consistent with migration of eolian dunes (Hunter, 1977a, 1977b; Kocurek and Dott, 1981).

4.2. Eolian depositional units and chronology

The presented nineteen stratigraphic sections with OSL ages are the basis for proposing a landscape evolution model comprised by six units of eolian strata interposed with paleosols and/or bounded by erosive surfaces, that represent phases of increased eolian sedimentation (Figs. 5 and 6; Table 3). These units were chronologically constrained by 61 OSL ages on quartz grains from eolian sands (Table 2) and are interpreted to represent six regionally significant eolian depositional phases (EDP) for the San Luis paleo-dune field during the past ca. 50 ka. These inferred eolian phases from youngest to oldest are 70 ± 10 yr (EDP 1a), 190 ± 20 yr (EDP 1b), ~12 to 1 ka (EDP 2), ~22 to 17 ka (EDP 3), ~29 to 24 ka (EDP 4) and ~40 to 32 ka (EDP 5), representing periods dominated by eolian sedimentation and separated by intervals of pedogenesis and/or hiatuses in deposition. EDP ages and errors are calculated as an unweighted mean with one sigma errors, except for EDP 2, which reflects the range of ages spanning the past ca. 12 ka (Table 3). The morphology of horizons for the paleosols is presented in Table 3. More details about Nueva Escocia and Blowout sections are in Tripaldi and Forman (2007); from Nicolas, Diego and Fede sections in Tripaldi et al. (2013); and from Esteban, Miguel, Tejon, Alfo, Quinto River overlook, Road cut A and Road cut B sections in Forman et al. (2014).

There is some uncertainty on the exact duration of these eolian depositional phases (EDP). This uncertainty is related to the current precision of OSL dating which for sediments >1000 years old are between 6 and 8.5% and for sediments that are ≤200 years old the errors are 7–14% (Wintle and Murray, 2006). The two youngest EDPs (1a and 1b) are historic phases. The oldest historic phase, EDP 1b, was identified at three sites with an average OSL age of 190 ± 20 years. This error reflects low number of ages (three) and thus, 40 years is a maximum estimate on the likely duration of EDP 1b. The most recent phase, EDP 1a, spanning the 1930s was subdecadal in scale. The timing and duration of this EDP (Tripaldi et al., 2013) is consistent with the unweighted mean and standard deviation for fourteen OSL ages of 72 ± 7 years (Table 2). EDP 2 is associated with eolian sand deposits that span a considerable period of time between ca. 12 and 1 ka with no identified paleosols or other major hiatus in the observed stratigraphy, and thus appears to be a nearly continuous accretion of a sand sheet deposit (Forman et al., 2014). In contrast, the three oldest EDPs are constrained by five or six OSL ages each and individual ages for EDPs 3, 4 and 5 overlap at one or two sigma errors and appear to be discrete phases. Therefore, the age range for EDP 3, 4 and 5 possibly reflects a measure of the duration of eolian deposition and also the intrinsic error in OSL dating. Until there is a larger population of ages (>10) from more sites and lower individual errors on OSL ages, the proposed duration of EDPs 3, 4 and 5 is probably a maximum estimate.

4.2.1. Eolian depositional phase 1a (EDP 1a)

EDP 1a represents the most recent eolian reactivation of the San Luis paleo-dune field that took place during the 20th century, with local to regional reactivation of dune forms (Tripaldi et al., 2013). Nine sections, widely distributed within the study area, show chronologically constrained deposits for this phase (Figs. 2, 5 and 6). Beneath many land surfaces there is a pedogenically unaltered, centimeter-to decimeter-thick cover of friable, well sorted, fine sand, that buries a recent soil and where these eolian sediments are absent the “paleosol” appears to merge with the surface soil. EDP 1a was characterized mostly by cross-bedded, moderately-well to well-sorted, fine to very fine sand associated with dune migration (Sp lithofacies; Table 1). Quartz grains from EDP 1a beds yielded 14 OSL ages between ~95 and ~60 yr (Figs. 5 and 6, Table 2). At the Esteban and Beto sections this eolian sand overlies conformably the Quizapú Ash derived from an historic eruption in AD 1932 (Hildreth and Drake, 1992). The mean of 13 OSL ages indicate eolian accumulation occurred at 72 ± 7 years ago (datum year AD 2000), which was concordant with a recorded 30–60% reduction in precipitation and historical observations of eolian

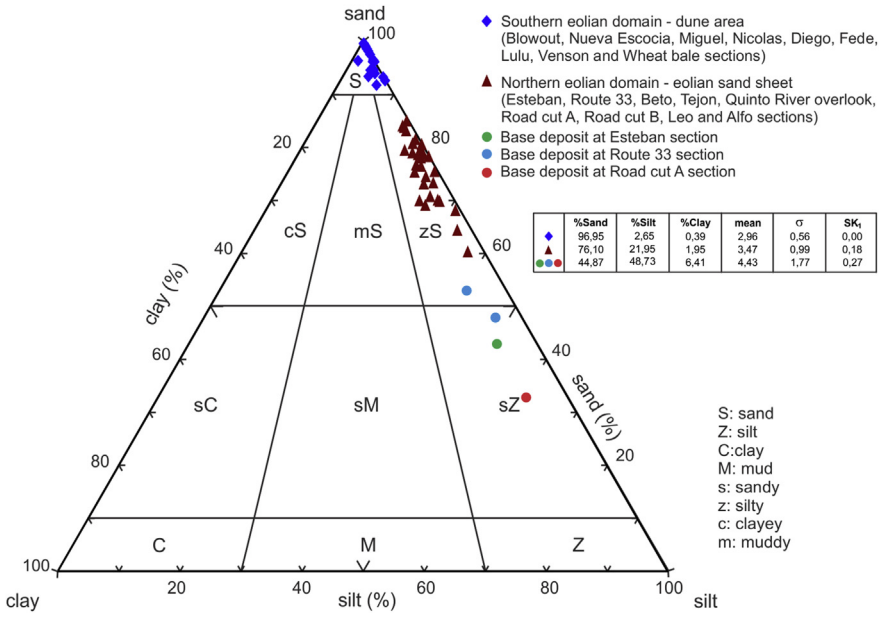

Fig. 4. Textural classification of eolian sediment of the San Luis paleo-dune field (after Folk et al., 1970), showing the two groups of sediments related to the northern and southern eolian domains and average values of some textural parameters (σ: sorting; SK_1: skewness).

activity during a severe drought in the 1930s, amplified by anthropogenic land surface disturbance (Tripaldi et al., 2013). A young age of 15 ± 1 yr from near surface sediments (UIC1609, Table 2) probably corresponds to recent landscape disturbance due to anthropogenic activities.

4.2.2. Eolian depositional phase 1b (EDP 1b)

Evidence for this historic phase was found in four separate localities, Tejon, Nicolas and Lulu sections, and possibly at the Fede section (Figs. 2, 5 and 6). At the Lulu site the EDP 1b massive, very well-sorted fine sand was separated from the overlying EDP 1 high angle cross-bedded sand, by a weak paleosol (A/C profile) (Table 3). At the Nicolas and Fede sections there was clear stratigraphic separation between the two most recent EDPs with high-angle cross beds of an EDP 1a sand burying horizontal to subhorizontal bedded EDP 1b deposit, characteristic of a sand sheet environment. Three OSL ages from these disparate sites indicate an age for EDP 1b of 190 ± 20 years (Table 2).

4.2.3. Eolian depositional phase 2 (EDP 2)

Several sites along the San Luis paleo-dune field reveal a nearly continuous succession of eolian sand that spanned most of the Holocene (Forman et al., 2014), and is here defined as EDP 2. This depositional phase partially reworked the late Pleistocene eolian cover deposits and resulted in the accumulation of ~3–6 m thickness of sand. These deposits are particularly extensive in the northern sand sheet area and are recognized at the Esteban, Beto, Tejon, Leo, Alfo, Miguel, Leo, Quinto River, Road cut A and Road cut B sections (Fig. 2). The sediments are composed of a silty sand, mostly massive or with diffuse, horizontal to low angle (<10°) laminations (SLm, SLh lithofacies, Table 1) (Figs. 4 and 5). Moreover, at Esteban and Beto sites the EDP 2 deposits are traced laterally for hundreds of meters, mirroring the present topography. EDP 2 is also recorded at the dune domain, at Miguel section with almost a 4-m-thick, moderately to well-sorted, fine sand with horizontal to very low angle cross-lamination (Sm, Sh lithofacies; Table 1) (Figs. 2 and 6). At this site the EDP 2 succession was bounded at the base and the top by paleosols (PM II and PM III, respectively; Table 3, Fig. 5), which separated it from the lower EDP 3 laminated sand and the upper more friable, massive sand of likely EDP 1 age. In three other sites the base of the EDP 2 successions was marked by an erosive surface that truncates a paleosol, with a calcareous argillic horizon (PQR I at Quinto River overlook, PRA I at Road cut A, PRB I at Road cut B, PL I at Leo and PA I at Alfo; Table 3, Figs. 2, 4 and 5). Twenty-seven OSL ages on quartz grains from EDP 2 beds indicate that eolian accumulation occurred between ca. 12 and 1 ka (Table 2, Figs. 5 and 6).

4.2.4. Eolian depositional phase 3 (EDP 3)

EDP 3 was mainly exposed in the dune domain at Beto, Route 33, Nueva Escocia, Miguel, and Wheat bale sections; and also recognized at the Tejon site as a sand sheet deposit (Fig. 2). This EDP was composed of a variety of eolian deposits including massive beds and units with horizontal and cross-bedded laminations (Figs. 5 and 6), fine-very fine to silty sand, representing accumulation by migration of eolian ripples (SLh, Sh lithofacies), dunes (Sp lithofacies) and suspension to modified saltation (SLm lithofacies; Table 1). The paleocurrent measurements of cross-bedding at the Wheat bale site indicate easterly paleowinds (mean dip direction to Azimuth 265°). The thickness of EDP 3 was generally modest, from ~1 m to 2.5 m. The upper boundary of this EDP was overprinted by a paleosol at Miguel section (PM II; Table 3, Fig. 5). This paleosol was also truncated by the emplacement of the overlying eolian sediment but retains a paleo-solum ~40–50 cm thick with carbonate morphologies and rubification (Table 3). In the Tejon section the exact thickness of EDP 3 deposits was unknown, but was probably <1 m and identified solely by the OSL age of 21,315 ± 1900 yr (UIC3279) (Fig. 5). At the Wheat bale site the EDP 3 deposit occurs at or near the surface covered by a thin layer of recent eolian sand (Fig. 6). The time constraint for EDP 3 was provided by six OSL ages on quartz grains from eolian beds from five sites, which yield an age range of ca. 22–17 ka (Fig. 5, Table 2). EDP 3 deposits with cross-bedding are associated with the large compound blowout dunes oriented by NE paleowinds. A preliminary and working hypothesis is that the compound/complex blowout dunes were developed during the late Pleistocene, and those oriented by NE paleowinds

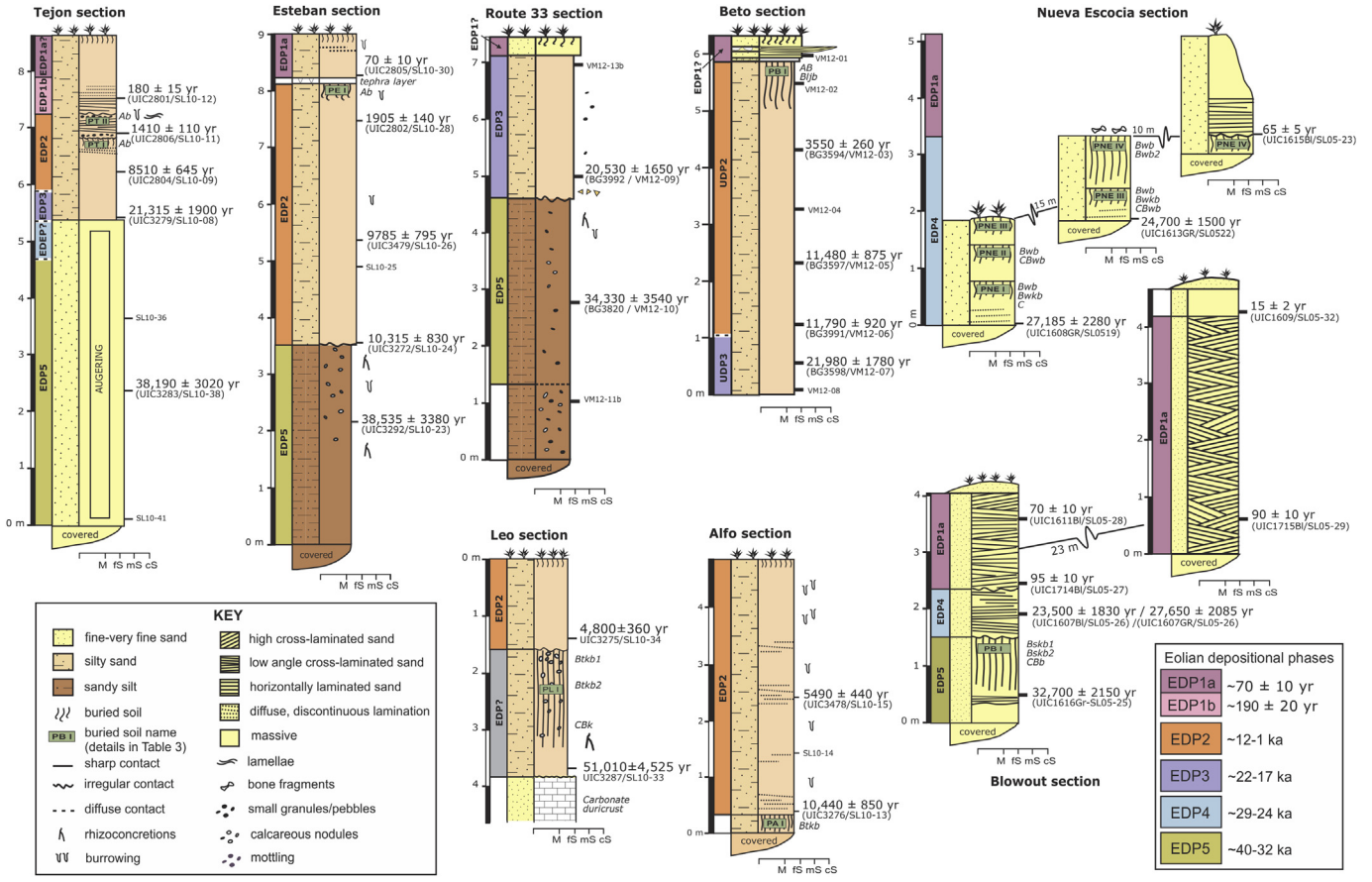

Fig. 5. Stratigraphic sections of the San Luis paleo-dune field showing bedding characteristics, buried soils with recognized horizons, OSL ages and eolian depositional phases (EDP) bounded by the buried soils and/or erosive surfaces. Section location: Tejon (33° 40.363′ S; 65° 22.950′ W), Esteban (33° 32.069′ S; 65° 19.876′ W), Route 33 (33° 27.505′ S; 65° 22.452′ W), Beto (33° 31.152′ S; 65° 20.225′ W), Nueva Escocia-Blowout (33° 49.197′ S; 65° 43.322′ W), Leo (33° 22.367′ S; 65° 34.609′ W), Alfo (33° 47.400′ S; 65° 22.713′ W).

are younger than those shaped by SE paleowinds and then possibly active during the EDP 3.

4.2.5. Eolian depositional phase 4 (EDP 4)

EDP 4 consists of 1-to-3-m thickness of horizontally-laminated, fine to very fine sand (Sh lithofacies in Table 1), indicating aggradation by eolian ripple migration. These deposits appear in the southern dune area, at Nueva Escocia, Blowout and Miguel sites (Figs. 5 and 6), where the landscape was formed by compound/complex blowout dunes and with recent eolian disturbance of the landscape (Fig. 2). At Miguel and Nueva Escocia sites the upper boundary of this unit was marked by a well-developed paleosol, with cambic and carbonate B horizon morphologies (PM I and PNE IV, respectively; Table 3, Figs. 4 and 5). The sand below this paleosol showed massive to diffuse laminated beds, likely due to pedogenic modifications. Quartz grains from the described beds yielded OSL ages of 27,700 ± 2100 yr (UIC2347) at Miguel site, 27,650 ± 2085 yr (UIC1607Gr) at Blowout site, and 27,185 ± 2280 yr (UIC1608GR) at Nueva Escocia site (Table 2; Fig. 5), indicating EDP 4 developed sometime between 29 and 24 ka. We interpret EDP 4 to represent part of the sedimentary record for accretion of the compound blowout dunes by SE paleowinds, thus these large landforms that characterize the San Luis paleo-dune field are, at least, ca. 28 ka old.

4.2.6. Eolian depositional phase 5 (EDP 5)

The most conspicuous characteristic of EDP 5 was the dominance of massive sandy silt to silty sand, commonly modified by pedogenesis with calcareous nodules, rhizoliths and burrow casts. EDP 5 appears at Esteban, Route 33 and Tejon sections, in the northern sand sheet domain, and at the Blowout section, located close to compound blowout dunes (Fig. 2). In the northernmost area the Esteban and Route 33 sections are composed of massive, sandy silt (LSm in Table 1, Fig. 4), interpreted as aggradation in a distal sand sheet or a sandy loessic environment. At Route 33, EDP 5 shows few (<1%) scattered, 1–5 cm diameter pebbles, mainly rounded clasts of andesite and some subrounded, carbonate-cemented clasts, features that suggest some alluvial reworking, possibly colluviated loess. To the south EDP 5 was represented by a very fine sand at the Tejon site and at the Blowout section by a massive to horizontally laminated, fine to very-fine sand (Sm, Sh in Table 1) (Fig. 4). Other likely deposits of eolian origin are exposed at the base of the Leo and Road cut A sections (SLm and LSm lithofacies, respectively), which comprise the C horizon of a well-developed paleosol (Figs. 5 and 6; Table 3). The thickness of EDP 5 was 1.5 m to at least 5 m, with the base often covered. The top of EDP 5 was pedogenically modified with well-developed argillic and pedogenic carbonate horizons at Blowout, Leo and Road cut A sections (PB I, PL I and PRA I, respectively; Figs. 5 and 6; Table 3). At Esteban and Route 33 sites this upper boundary was marked by an erosive surface, but the presence of common calcareous nodules, rhizoliths and burrow casts indicate a remnant paleosurface, which was eroded. At the Tejon site the top of EDP 5 deposit was not sufficiently exposed because the lower part of this section was sampled by auguring. OSL dating of quartz grains from EDP 5 yielded an age range of ~40 to 32 ka (Table 2, Figs. 5 and 6). The basal deposit of Leo section dated to 51,010 ± 4525 yr (UIC3287,

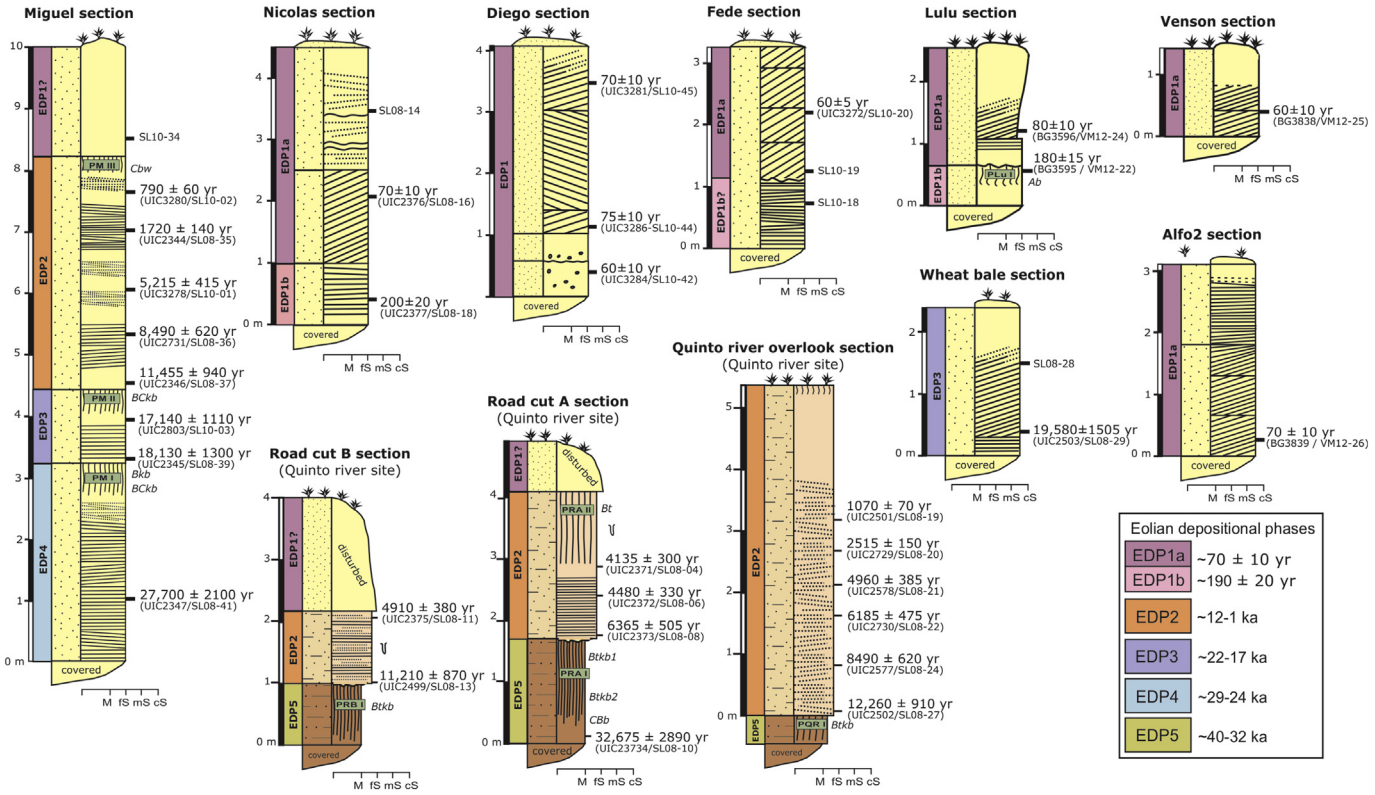

Fig. 6. Stratigraphic sections of the San Luis paleo-dune field showing bedding characteristics, buried soils with recognized horizons, OSL ages and eolian depositional phases (EDP) bounded by the buried soils and/or erosive surfaces. Section location: Miguel (33° 58.341′ S; 65° 35.298′ W), Nicolas (33° 51.215′ S, 65° 24.290′ W), Diego (33° 08.535′ S, 65° 21.773′ W), Fede (33° 58.049′ S, 65° 34.550′ W), Lulu (34° 20.516′ S; 65° 39.516′ W), Venson-Alfo 2 (34° 7.509′ S; 65° 21.890′ W), Wheat bale (34° 8.024′ S; 65° 23.188′ W), Quinto River overlook (33° 50.333′ S; 65° 14.669′ W), Road cut A (33° 50.353′ S; 65° 14.619′ W), Road cut B (33° 50.353′ S; 65° 14.584′ W).

Table 2) may represent an older episode of eolian sedimentation.

5. Discussion

5.1. Relation between San Luis eolian depositional phases and other eolian records in central Argentina

We infer correlations with other eolian stratigraphic records in the region to test the robustness of the EDPs defined for San Luis Province. Stratigraphic sections within the Médanos de los Naranjos dune field in the Andean piedmont (Fig. 1) expose intercalated eolian, volcanic, and fluvial deposits. A variety of fluvial and eolian sedimentary facies were recognized and eleven OSL ages on quartz grains provided chronologic control, though six ages were determined on twelve or less aliquots (Tripaldi et al., 2011), which may not reflect robust equivalent dose populations, particularly with overdispersion values unreported (cf. Roberts et al., 1999; Galbraith and Roberts, 2012). Facies 1 sediment at the base of ACH2 section reflects variable eolian-fluvial deposition; a sandy eolian bed yielded a single OSL age of 32.50 ± 3.41 ka (UGA08OSL-529; Tripaldi et al., 2011). It is uncertain if this facies reflects broader eolian deposition across the landscape. Eolian deposits were ubiquitous near the surface with fine sand with planar, low and high-angle cross beds reflecting dune migration and sand sheet accretion. At ACH2 section, eolian beds yielded OSL ages of 21.18 ± 1.47 ka (UGA07OSL-504), 21.16 ± 1.54 ka (UGA07OSL-503), and 19.06 ± 1.72 ka (UGA07OSL-502), that may be correlative with EDP 3 (Fig. 7). The eolian facies exposed at ACH1 section returned bounding OSL ages of 14.17 ± 1.35 ka (UGA07OSL-499) and 1.61 ± 0.21 ka (UGA07OSL-500), and may be partially correlative to EDP 2.

Two other dune fields on the Andean piedmont exhibit evidence for eolian activity, but only during the late Holocene (Tripaldi and Forman, 2007), and may relate in part to EDP 2 (Fig. 7). In the Médanos Grandes dune field (Fig. 1) a natural section exposes the internal stratigraphy of a linear dune, with eolian cross-bedding and associated OSL ages on quartz grains between ca. 4.3 and 4.0 ka (Tripaldi and Forman, 2007). A second section in this dune field shows eolian beds that bury alluvial fan deposits and yielded OSL ages of 2070 ± 150 yr (UIC1719Bl), 600 ± 40 yr (UIC1615Bl), 400 ± 45 yr (UIC1617Bl) and 410 ± 45 yr (UIC1612Bl; Tripaldi and Forman, 2007), revealing a landscape with recurrent episodes of eolian sedimentation. This dune field is located currently in the driest region of central Argentina (MAP = 91 mm; Compagnucci et al., 2002) and may reflect heightened sensitivity to regional aridity or sediment source variability. The Médanos Negros paleo-dune field in La Rioja Province (Fig. 1), with a mean annual precipitation of ~370 mm, exhibits eolian aggradation at ca. 2.5 and 0.9 ka (Tripaldi and Forman, 2007), which may be correlate in part to EDP 2 (Fig. 7). Eolian sedimentation ca. 400 years ago was also identified in this dune field, similar to Médanos Grandes dunefield (Tripaldi and Forman, 2007).

To the east of the San Luis paleo-dune field the eolian deposit continues, with several meter-thick sand sheet sediments. A stratigraphic section cut by the Arroyo Las Lajas in Córdoba Province (Fig. 1) exposes more than 11 m of fluvial and eolian deposits with interposed buried soils. The two upper sandy units, formally named La Invernada and Laguna Oscura formations, are separated by a paleosol, and considered to be eolian in origin, with fluvial beds at the base (Degiovanni et al., 2005 and references therein).

Table 3
Soil-stratigraphic descriptions for study sites San Luis Province, western Pampas, Argentina.

Paleosol/Section	Horizon	Depth (cm)	Boundary[a]	Texture[b]	Color	Structure[c]	Effervescent[d]	Other features
PA I/Alfo	Btkb	0–20+	–	CL	7.5YR 4/6	4msbk	VE	Stage 2 $CaCO_3$ nodule
PB I/Blowout	Bskb1	0–50	gs	vfSa	10YR 4/3.5	2–3msbk	NE	Rhizoliths, Fe mottling (7.5YR 4/5)
	Bskb2	50–70	cs	vfSa	10YR 4/5	2–3msbk	NE	Fe mottling (7.5YR 4/3)
	CBb	70–100	gs	vfSa	7.5YR 4/4	1–2fsbk	NE	
PL I/Leo	Btkb1	0–30	gs	CL	7.5YR 4.5/6	4msbk	VE	Stage 2 $CaCO_3$ nodule
	Btkb2	30–95	gs	SICL	7.5YR 5/6	3msbk	VE	
	CBk	95–170	–	SvfSa	7.5YR 4/4	2msbk	ST	$CaCO_3$ rhizoliths
PM I/Miguel	Bkb	0–31	cs	SImSa	10YR 3.5/3	3msbk	VE	Stage 1 filamentous $CaCO_3$
	CBk	31–48	gs	mSa	10YR 3.5/3	2msbk	ST	
PM II	CBk	0–30	gw	mSa	10Y4 5/4	2msbk	ST	Filamentous $CaCO_3$
PM III	Cwb							
PNE I/Nueva Escocia	Bwb	0–32	cs	SvfSa	10YR 4/3	2–3msbk	NE	
	Bwkb	32–55	cs	SvfSa	10YR 4.5/3	1–2fsbk	WE	$CaCO_3$ rhizoliths
	C	55–75	–	vfSa	10YR 5/4	1fsbk	NE	
PNE II	Bwb	0–15	gs	SvfSa	10YR 4/3	1–2fsbk	NE	
	CBw	15–28	–	vfSa	7.5YR 4.5/4	1fsbk	NE	
PNE III	Bwb	0–55	gs	SvfSa	10YR 4.5/4	3msbk	NE	
	Bwkb	55–75	gs	SvfSa	10YR 3.5/4	4 msbk	WE	
	CBw	75–93	gs	vfSa	10YR 4/6	2msbk	NE	
	C	93-	–	vfSa	7.5YR 4/3	1fsbk	NE	
PNE IV	Bwb1	0–45	gs	SvfSa	10YR 5/4	3msbk	NE	Abundant small bones, rodent teeth and jaws on top
	Bwb2	45–60	gs	vfSa	7.5YR 5/4	1–2fsbk	NE	
PRA I/Road cut A	Btk	0–95	–	SICL	7.5YR 4/6	4msbk	ST	Abundant clay skins
PRA II	Btk1	0–105	gs	SICL	5.5YR 4/5	3msbk	ST	Abundant clay skins
	Btk2	105–145	gs	SICL	5YR 4/4, 5YR 5/4	2mabk	ST	Common clay skins
	BC	145–180	–	L	10YR4/3	1mabk	NE	
PRB I/Road cut B	Btk1	0–95	gs	SICL	5.5YR 4/5	3msbk	ST	Abundant clay skins
PE I/Esteban	Ab	1–15	gs	vfSa	10YR 4/2	sg	NE	
PB I/Beto	Ab	0–15	gs	SvfSa	10YR 5/2	4cabk	NE	
	Bljb	15–25	gs	SvfSa	10YR 5/3	2msbk	NE	
PLu I/Lulu	Ab	1–15	ws	vfSa	10YR 4/3	sg	NE	
PT I/Tejon	Ab	0–30	gs	vfSa	10YR 3.5/10YR4/4	sg	NE	
PT II	Ab	0–10	gs	vfSa	10YR 3/3	sg	NE	

[a] g-gradual, c-clear, a-abrupt; s-smooth, w-wavy.
[b] mSa-medium sand, vfSa-very fine sand, SImSa-Silty medium sand, SvfSa-Silty very fine sand, L-loam, SCL-sandy clay loam, SIL-silt loam, SICL-silty clay loam, CL-clay loam.
[c] 1-weak, 2-moderate, 3-strong; f-fine, m-medium, c-coarse; sbk-subangular blocky, abk-angular blocky, pr-prismatic, sg-single grained.
[d] NE-noneffervescent, WE-weakly effervescent, ST-strongly effervescent, VE-very strongly effervescent.

Six ages by both thermoluminescence (TL) and infrared stimulated luminescence (IRSL) constrain the timing of eolian deposition, though there was no information about the dating protocol used (Degiovanni et al., 2005). Two stratigraphic levels of La Invernada Formation yielded ages of 17.2 ± 1.6 ka (TL) and 18.4 ± 1.2 ka (IRSL) for the lower part, and 12.8 ± 1.5 ka (TL) and 16.2 ± 1.1 ka (IRSL) for the upper part, that may be correlative to EDP 3 (Fig. 7). An extensive near-surface eolian fine sand (Laguna Oscura Formation), buried the Las Tapias Geosol and reflects broader eolian deposition across the landscape. Eolian beds near the top of this succession yielded ages of 3.7 ± 0.6 ka (TL) and 4.2 ± 0.8 ka (IRSL) (Degiovanni et al., 2005), which may be partially correlative to EDP 2.

The Pampean loess record extends throughout the late Pleistocene showing multiple loess units separated by complex paleosols (Kemp et al., 2004, 2006; Zárate, 2007; Zárate et al., 2000, 2009; Heil et al., 2010). Two localities on the western Pampas, Monte Ralo and Corralito sites (Fig. 1) expose loess and loessoid successions with interposed buried soils that reflect distinct periods of eolian sedimentation on the western Pampas during the past ca. 150 ka (Frechen et al., 2009). These sequences were dated by TL and IRSL on the polymineral fine-grained fraction; the latter in other studies have yielded inconsistent, underestimates in age (cf. Spooner, 1994; Huntley and Lamothe, 2001; Roberts, 2012). In this study the error associated with TL and IRSL ages was variable between 9 and 34%. At the Corralito site the pre-penultimate period of loess deposition was constrained by two IRSL ages of 66.1 ± 9.4 ka and 32.5 ± 5.6. The penultimate period of loess deposition appears to date from ca. 19 to 13 ka, though there was one inconsistent IRSL age of 32.7 ± 6.7 ka. At the Monte Ralo site there are three stacked paleosols developed in loess and reworked loess which yielded the ages of ca. 77, 68, and 47 to 28 ka (Frechen et al., 2009); additional stratigraphic and chronologic analyses is needed to fully vet this record.

In the eastern Pampas, at the Tortugas section (Fig. 1), loess and loessoid succession was exposed, partially modified by pedogenesis, and returned OSL ages of 63.2 ± 3.4 ka (GL02004), 57.6 ± 2.9 ka (GL02003) and 23.3 ± 1.4 ka (GL02002; Kemp et al., 2004). This record appears to predate EDP 5 and with just one younger age (23.3 ka). In contrast, Kemp et al. (2004) interpreted that the deposition of the loess at Tortugas site likely extended into the Holocene according to an OSL age of 1.0 ± 0.1 ka at the section top (GL02001; Kemp et al., 2004) and a previous TL age of 8.1 ± 0.4 ka (Kröhling, 1999) and may correspond with EDP 2 (Fig. 7). There are three other loess records on the eastern Pampas, at the Baradero, Gorina and Hudson sites (Fig. 1), where the loess was modified significantly by pedogenesis. OSL ages from C horizon levels reveal loess accumulation spanned between ca. 56 ka and 40 ka, and ca. 27 and 23 ka (Kemp et al., 2004; Zárate et al., 2009), the later may be coeval with EDP 3 (Fig. 7), though chronologic control was limited.

5.2. Environmental and climatic significance of eolian deposition

The main factors that control the transport of eolian sand are wind speed, sand supply and availability (cf. Kocurek and Lancaster, 1999). The San Luis paleo-dune field constitutes a predominately availability-controlled eolian system, where there was a large

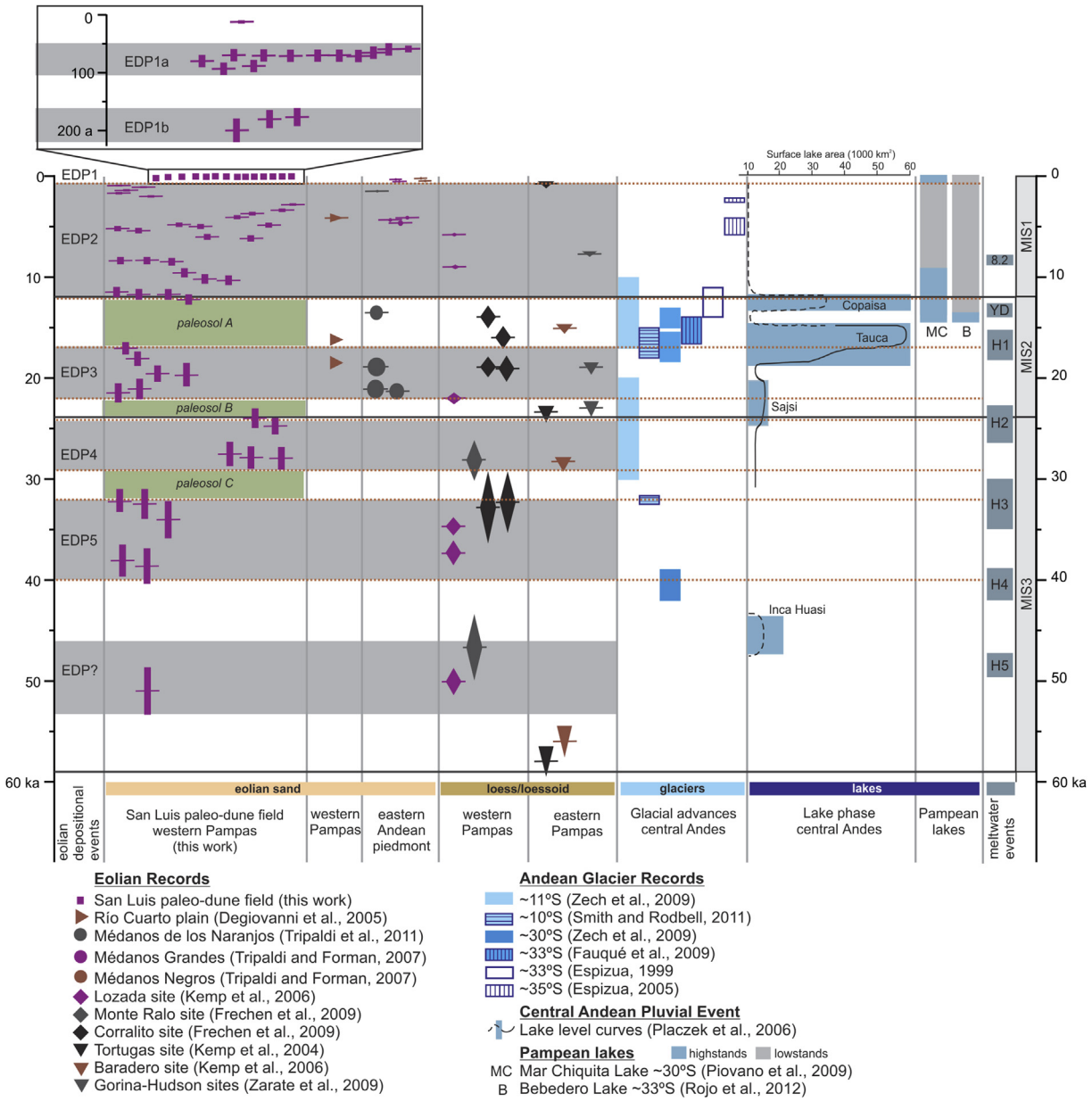

Fig. 7. Comparison of the eolian depositional phases (EDP) of the San Luis paleo-dune field (western Pampas, Argentina) with other Quaternary record of eolian sand of western Pampas and Andean piedmont, loess and loessoid deposits of western and eastern Pampas, glacier advances in the central Andes and lake phases from central Andes and Pampas. Meltwater events in grey (H, Heinrich events; YD, Younger Dryas; 8.2, 8.2 ka event). The horizontal line marks the eolian age and the symbol height reflects the age error.

supply of well sorted, fine sand at the surface, beneath grassland and with common threshold wind speeds (>5 m/s) for sand movement attained seasonally (Tripaldi and Forman, 2007; Forman et al., 2014). At present, the extensive Espinal grassland reflects a mean annual precipitation of ~750 mm which limits eolian activity with only minor eolian transport related to local anthropogenic disturbance. However, there was widespread dune reactivation and eolian deposition in the 1930s in the San Luis paleo-dune field in response to a 30–60% reduction in mean annual precipitation and amplified by anthropogenic factors (Tripaldi et al., 2013).

Sediment transport in continental dune fields is inversely proportional to vegetation cover and soil moisture and directly dependent on local wind speed (cf. Lancaster, 1988; Houser et al., 2015). Thus, an annual rainfall of about 250 mm is considered generally the upper limit for active dunes at inland dune fields (Pye and Tsoar, 2009: 153) and eolian transport is limited severely when the vegetation cover exceeds 30% (Ash and Wasson, 1983; Kuriyama et al., 2005). Here we interpret the identified eolian depositional phases (EDP) consistent with conceptual and quantitative models of eolian instability (Lancaster, 1988; Muhs and Holliday, 1995; Houser et al., 2015), as periods of increased sand availability in response to a decrease in vegetation cover and soil moisture under the ambient wind field, which reflects a substantial reduction in effective precipitation. Previously, the dominance of sand sheet sedimentation between ca. 12 and 1 ka, associated with EDP 2, was inferred to reflect an ecotone shift from Espinal savannah to Monte shrub steppe, with a mean annual precipitation between 450 and 100 mm, which was considerably drier than the late 20th century average of ~750 mm (Forman et al., 2014). In contrast, periods of increased precipitation favored a more extensive vegetation cover

and higher soil moisture, which may have reduced eolian activity, promoting landscape stability and pedogenesis. Therefore, we interpreted the presence of eolian units bounded by buried soils as alternating changes in moisture availability and vegetation cover, and, at the extreme response, may have reflected an ecotone shift from Espinal to Monte.

Currently, the majority of moisture is delivered during the spring and summer by the low level meridional Chaco Jet, due to the influence of the South American Monsoon system in the western Pampas (Silva and Kousky, 2012). Several paleoclimatic studies of the tropical-subtropical South America infer significant changes in moisture availability with intensification and/or southward shift of the SAMS, controlled by the southerly displacement of the ITCZ (Sylvestre et al., 1999; Trauth and Strecker, 1999; Baker et al., 2001; Cruz et al., 2006; Sylvestre, 2009; Blard et al., 2011). Recently, the discovery of abrupt methane increases in a Greenland ice core through Heinrich events 1, 2, 4, and 5 and intervening periods has been linked to an intensification of the Southern Hemisphere monsoonal rainfall across Africa, Asia and South America (Rhodes et al., 2013). Thus, we infer the resultant variable moisture conditions also affect the western Pampas with drier intervals associated with eolian deposition and sand sheet accretion, within a possible Monte-type ecotone, while intervening periods of pedogenesis associated with increased effective moisture and vegetation density, perhaps similar to the current Espinal ecotone; and reflect increased intensity of the SAMS (cf. Forman et al., 2014).

The periods of pedogenesis at ca. 17 to 12 ka, 24 to 22 ka, and 32 to 29 ka (paleosols A, B and C in Fig. 7), are inferred to be wetter episodes in western Argentina and may have coincided with high lake stands, and glaciations in the adjacent high Andes (cf. Placzek et al., 2009; Blard et al., 2011). The latest period of pedogenesis between 17 and 12 ka is broadly coincident with last two lake high stands, Tauca and Coipasa, between 18 and 11 ka (Fig. 7). However, there is less certainty if the earlier two episodes of pedogenesis correspond with lake high stands because of limited chronologic control (Fig. 7). In turn, the relation of these intervals of pedogenesis to glacier advances in the central Andes during the late Pleistocene is unclear, reflecting recent refinements in the production rate for ^{10}Be in the high tropical Andes (Blard et al., 2013) and apparent broad age range of some glacial periods (Fig. 7), though glacier extent appears to be primarily precipitation-controlled (Kull and Grosjean, 2000). Many studies yielded ^{10}Be ages on glacial erratics between 18 and 10 ka (Espizúa, 1999, 2005; Fauqué et al., 2009; Zech et al., 2009; Smith and Rodbell, 2010), which broadly coincide with paleosol 1 and high Andean lake levels during Heinrich Event 1 and the Younger Dryas chronozone (Fig. 7). Older cosmogenic ^{10}Be ages on glacial erratics from moraines yielded age ranges of 42 to 39 ka and 32 to 20 ka (Zech et al., 2009; Smith and Rodbell, 2010) (Fig. 7), with the latter period possibly coincident with all or part of the time span for paleosols b and c (Fig. 7). Carbon and strontium isotopic analyses on carbonate for the latest high stands for Altiplano lakes indicate that moisture is derived from the eastern side of the Andes, associated with the southward displacement of the ITCZ with Northern Hemisphere Heinrich events (Placzek et al., 2006, 2011; Blard et al., 2011; Hemming, 2004). Sediment records from the Pampean Desaguadero and Mar Chiquita lakes, also show highstands during the transition from the late Pleistocene to the Holocene linked to enhanced moisture transport from Atlantic Ocean sources, though chronologic control is limited (Piovano et al., 2009; Rojo et al., 2012) (Fig. 7).

There is compelling evidence from the San Luis paleo-dune field for nearly continuous sand sheet deposition ca. 12 to 1 ka associated with EDP 2, which broadly overlaps with other eolian records from central Argentina, though with limited chronologic control (Degiovanni et al., 2005; Tripaldi et al., 2011) (Fig. 7). There are six OSL ages from the basal 10 cm of the sand sheet deposit associated with the commencement of EDP 2 of 11,210 ± 870 yr (Road cut B; UIC2499), 12,260 ± 910 yr (Quinto River overlook; UIC2502), 11,455 ± 940 yr (Miguel; UIC2803), 11,480 ± 875 yr (Beto; BG3598), 10,440 ± 850 yr (Alfo; UIC3276); 10,315 ± 830 year (Esteban; UIC3272); the unweighted mean is 11,190 ± 450 yr, which corresponds to the end of the Younger Dryas (at one sigma errors), with widespread drying across subtropical South America (Placzek et al., 2011; Blard et al., 2011). The end of sand sheet deposition is less certain because of the development of a soil in the upper 50 cm of the sand sheet. The youngest secure age on termination of sand sheet deposition was from the Miguel site with an OSL age of 790 ± 60 yr (UIC3282) on quartz grains from 55 cm below the unit top. Recent lake coring results at the Nassau lake in the study area may reflect climatic amelioration since ca. 900 cal yr BP (Vilanova et al., 2015; Figs. 1 and 2).

The two youngest EDPs (1a and 1b) occurred at 70 ± 10 yr and 190 ± 20 yr ago. There is widespread evidence that the latest phase, EDP 1a, occurred in the 1930s with local reactivation of dunes and in places conformable deposition of a sand sheet deposit over the Quizapú Ash, deposited from a volcanic eruption in AD 1932 (Tripaldi et al., 2013). The spatial distribution of the penultimate phase (EDP 1b) is unknown with only four recognized sites. Historic wetland and river discharge observations near Mendoza in western Argentina indicates a particular wet period between AD 1670 and 1860 (Prieto et al., 2008; Prieto and Rojas, 2012), possibly associated with regional deforestation (cf. Woodward et al., 2014). Thus, eolian deposition may reflect initial European landscape disturbance with overgrazing by cattle and horses in the late 18th century (cf. E. Jobbagy, pers. com. May, 2015).

6. Conclusions

The sedimentary record of the subtropical San Luis paleo-dune field reveals a succession of eolian deposits spanning the past 50 ka. Nineteen disparate stratigraphic sections over about 7500 km^2 exhibit discrete eolian depositional phases often bounded by buried soils or erosive unconformities. Sixty two OSL ages on quartz grains from this stratigraphic setting are the basis for inferring six eolian depositional phases, termed from youngest to oldest EDP 1 to EDP 5. The timing of these eolian phases were at ca. 70 ± 10 yr, 190 ± 20 yr, 12 to 1 ka, 22 to 17 ka, 29 to 24 ka and 40 to 32 ka. Bounding OSL ages provide maximum estimates for the periods of pedogenesis of 12–17 ka, 22 to 24, and 29 to 32 ka; the youngest period overlaps *sensu lato* with wetter intervals in the late Pleistocene, during high stands of pluvial lakes and glacial advances in the central Andes and appear linked with Northern Hemisphere Heinrich events (cf. Placzek et al., 2009; Blard et al., 2011). The older periods of pedogenesis coincide with Heinrich Events 2 and 3 and possibly glaciation events in the central and northern Andes, but chronologic control is limited (Zech et al., 2009; Smith and Rodbell, 2010). EDP 2 commences at 11.2 ± 0.45 ka, coincides with the end of the Younger Dryas epoch and spans most of the Holocene to ca. 700 years ago. Eolian sedimentation for EDP 2 was characterized by sand sheet accretion and was associated with a Monte ecotone and an inferred mean annual precipitation of 100–450 mm, drier conditions compared to the late 20th century.

The most pervasive eolian deposit (EDP 1a) in San Luis Province is sand sheet and dune sediments associated with drought conditions and anthropogenic landscape disturbance in the 1930s. An earlier EDP 1b at ca. 190 years ago was recognized in a few sites and may reflect heterogeneous landscape disturbance in response to overgrazing with European settlement and during a particularly

wet period. At present, there is limited eolian activity in the western Pampas with excess of surface waters forming new lakes and rivers; a response to the spread of agriculture, replacing the Espinal vegetation, and wetter climatic conditions since the 1970s.

Acknowledgements

The authors' gratitude is extended to able field assistance from H. Reinjestein, A. Quesada, T. Luppo, J. Perelló, P. Ciccioli, P. Forte, F. González Tomassini, N. Kubik, L. Marín, and T. Badger. Meteorological data were kindly provided by the Servicio Meteorológico Nacional (National Weather Service). Funding for this research was supported by Universidad de Buenos Aires (UBACyT20620100100009 and UBACyT20620130100002BA) and CONICET fellowship to AT; and National Geographic Society Grant 8607-09 to SLF. Assistance in OSL dating was provided by J. Mazzoco, J. Pierson and L. Marín. The comments of the two journal reviews and the editor are highly appreciated. We are grateful to the many farmers and ranchers of San Luis Province whose generosity and hospitality made this study possible.

Appendix A. Supplementary data

Supplementary data related to this article can be found at http://dx.doi.org/10.1016/j.quascirev.2016.03.007.

References

Abbott, M.B., Wolfe, B.B., Wolfe, A.P., Seltzer, G.O., Aravena, R., Mark, B.G., Polissar, P.J., Rodbell, D.T., Rowe, H.D., Vuille, M., 2003. Holocene paleohydrology and glacial history of the central Andes using multiproxy lake sediment studies. Palaeogeogr. Palaeoclimatol. Palaeoecol. 194 (1–3), 123–138.

Abraham, E., del Valle, H.F., Roig, F., Torres, L., Ares, J.O., Coronato, R., Godagnone, R., 2009. Overview of the geography of the Monte desert biome (Argentina). J. Arid Environ. 73, 144–153.

Andreoli, R.V., Kayano, M.T., 2005. ENSO-related rainfall anomalies in South America and associated circulation features during warm and cold Pacific decadal oscillation regimes. Int. J. Climatol. 25 (15), 2017–2030.

Ash, J.E., Wasson, R.J., 1983. Vegetation and sand mobility in the Australian desert dunefield. Z. Geomorphol. 45, 7–25.

Baker, P.A., Rigsby, C.A., Seltzer, G.O., Fritz, S.C., Lowenstein, T.K., Bacher, N.P., Veliz, C., 2001. Tropical climate changes at millennial and orbital timescales on the Bolivian Altiplano. Nature 409, 698–700.

Barros, V.R., Doyle, M.E., Camilloni, I.A., 2008. Precipitation trends in southeastern South America: relationship with ENSO phases and with low-level circulation. Theor. Appl. Climatol. 93, 19–33.

Birkeland, P.W., 1999. Soils and Geomorphology, third ed. Oxford University Press, New York, p. 430.

Blard, P.H., Braucher, R., Lave, J., Bourles, D., 2013. Cosmogenic ^{10}Be production rate calibrated against ^{3}He in the High Tropical Andes (3800-4900 m, 20-22° S). Earth Planet. Sci. Lett. 382, 140–149.

Blard, P.H., Sylvestre, F., Tripati, A.K., Claude, C., Causse, C., Coudrain, A., Condom, T., Seidel, J.L., Vimeux, F., Moreau, C., Dumoulin, J.P., Lavé, J., 2011. Lake highstands on the Altiplano (Tropical Andes) contemporaneous with Heinrich 1 and the Younger Dryas: new insights from ^{14}C, U-Th dating and δ^{18}O of carbonates. Quat. Sci. Rev. 30 (27–28), 3973–3989.

Boggs Jr., S., 2006. Principles of Sedimentology and Stratigraphy, fourth ed. Pearson Prentice Hall, p. 662.

Cabrera, A.L., 1976. Regiones fitogeográficas argentinas. Enciclopedia Argentina de Agricultura y Jardinería, second ed., Tomo II, pp. 1–85 fasc. 1.

Clapperton, C., 1993. Quaternary Geology and Geomorphology of South America. Elsevier, Amsterdam, p. 779.

Contreras, S., Santoni, C.S., Jobbágy, E.G., 2013. Abrupt watercourse formation in a semiarid sedimentary landscape of central Argentina: the roles of forest clearing, rainfall variability and seismic activity. Ecohydrology 6 (5), 794–805.

Compagnucci, R.H., Agosta, E.A., Vargas, W.M., 2002. Climatic change and quasi-oscillations in central-west Argentina summer precipitation: main features and coherent behaviour with southern African region. Clim. Dyn. 18 (5), 421–435.

Crouvi, O., Amit, R., Enzel, Y., Gillespie, A.R., 2010. Active sand seas and the formation of desert loess. Quat. Sci. Rev. 29, 2087–2098.

Cruz Jr., F.W., Burns, S.J., Karmann, I., Sharp, W.D., Vuille, M., 2006. Reconstruction of regional atmospheric circulation features during the late Pleistocene in subtropical Brazil from oxygen isotope composition of speleothems. Earth Planet. Sci. Lett. 248, 495–507.

Degiovanni, S., Villegas, M., Blarasin, M., Sagripanti, G., 2005. Hoja Geológica Río Cuarto- 3263-III Secretaria de Minería de la Nación - Servicio Geológico Minero Argentino, p. 95. Buenos Aires.

Doyle, M., Barros, V., 2002. Midsummer low–level circulation in subtropical South America and related precipitation patterns. J. Clim. 15, 3394–3410.

Duller, G.A.T., 2003. Distinguishing quartz and feldspar in single grain luminescence measurements. Radiat. Meas. 37, 161–165.

Durcan, J.A., Duller, G.A.T., 2011. The fast ratio: a rapid measure for testing the dominance of the fast component in the initial OSL signal from quartz. Radiat. Meas. 46 (10), 1065–1072.

Espizúa, L., 1999. Chronology of late Pleistocene glacier advances in the Ro Mendoza Valley. Argentina. Glob. Planet. Change 22 (1), 193–200.

Espizúa, L., 2005. Holocene glacier chronology of Valenzuela Valley, Mendoza Andes, Argentina. Holocene 15 (7), 1079–1085.

Fain, J., Soumana, S., Montret, M., Miallier, D., Pilleyre, T., Sanzelle, S., 1999. Luminescence and ESR dating-beta-dose attenuation for various grain shapes calculated by a Monte-Carlo method. Quat. Sci. Rev. 18, 231–234.

Fauqué, L., Hermanns, R., Hewitt, K., Rosas, M., Wilson, C., Baumann, V., Lagorio, S., Di Tommaso, I., 2009. Mega-deslizamientos de la pared sur del cerro Aconcagua y su relación con depósitos asignados a la glaciación pleistocena. Rev. Asoc. Geol. Argent. 65, 691–712.

Folk, R.L., Andrews, P.B., Lewis, S.W., 1970. Detrital sedimentary rock classification and nomenclature for use in New Zealand. N. Z. J. Geol. Geophys. 13, 937–968.

Folk, R.L., Ward, W.C., 1957. Brazos river bar – a study in the significance of grain-size parameters. J. Sediment. Petrol. 27 (1), 3–27.

Forman, S.L., Oglesby, R., Markgraf, V., Stafford, T., 1995. Paleoclimatic significance of Late Quaternary eolian deposition on the piedmont and high plains, central United States. Glob. Planet. Change 11, 35–55.

Forman, S.L., Tripaldi, A., Ciccioli, P.L., 2014. Eolian sand sheet deposition in the San Luis paleodune field, western Argentina as an indicator of a semi-arid environment through the Holocene. Palaeogeogr. Palaeoclimatol. Palaeoecol. 411, 122–135.

Frechen, M., Seifert, B., Sanabria, J.A., Argüello, G.L., 2009. Chronology of late Pleistocene Pampa loess from the Córdoba area in Argentina. J. Quat. Sci. 24, 761–772.

Galbraith, R., Green, P., 1990. Estimating the component ages in a finite mixture. Int. J. Radiat. Appl. Instrum. Part D. Nucl. Tracks Radiat. Meas 17 (3), 197–206.

Galbraith, R.F., Roberts, R.G., 2012. Statistical aspects of equivalent dose and error calculation and display in OSL dating: an overview and some recommendations. Quat. Geochronol. 11, 1–27.

Galbraith, R.F., Roberts, R.G., Laslett, G.M., Yoshida, H., Olley, J.M., 1999. Optical dating of single and multiple grains of quartz from Jinmium rock shelter, northern Australia, part 1, experimental design and statistical models. Archaeometry 41, 339–364.

Garreaud, R.D., Vuille, M., Compagnucci, R., Marengo, J., Villalba, R., Grosjean, M., Kiefer, T., 2009. Present-day South American climate. Palaeogeogr. Palaeoclimatol. Palaeoecol. 281 (3–4), 180–195.

Grimm, A.M., 2003. The El Niño impact on the summer monsoon in Brazil: regional processes versus remote influences. J. Clim. 16, 263–280.

Heil Jr., C.W., King, J.W., Zárate, M.A., Schultz, P.H., 2010. Climatic interpretation of a 1.9 Ma environmental magnetic record of loess deposition and soil formation in the central eastern Pampas of Buenos Aires, Argentina. Quat. Sci. Rev. 30, 1–14.

Heinrich, H., 1988. Origin and consequences of cyclic ice-rafting in the northeast Atlantic Ocean during the past 130,000 years. Quat. Res. 29, 142–152.

Hemming, S.R., 2004. Heinrich events: massive late pleistocene detritus layers of the North Atlantic and their global climate imprint. Rev. Geophys. 42, 1–43.

Hildreth, W., Drake, R.E., 1992. Volcan Quizapú, Chilean Andes. Bull. Volcanol. 54, 93–125.

Houser, C., Bishop, M.P., Barrineau, P., 2015. Characterizing instability of aeolian environments using analytical reasoning. Earth Surf. Process Landf. 40 (5), 696–705.

Hunter, R.E., 1977a. Basic types of stratification in small eolian dunes. Sedimentology 24, 361–387.

Hunter, R.E., 1977b. Terminology of cross-stratified sedimentary layers and climbing-ripple structures. J. Sediment. Petrol. 47, 697–706.

Huntley, D.J., Lamothe, M., 2001. Ubiquity of anomalous fading in K-feldspars and the measurement and correction for it in optical dating. Can. J. Earth Sci. 38, 1093–1106.

Iriondo, M., 1990. The map of the South American plains. Its present state. Quat. S. Am. Antarct. Penins. 6, 297–306.

Iriondo, M., 1999. Climatic changes in the South American plains: records of a continent-scale oscillation. Quat. Int. 57–58, 93–112.

Iriondo, M., Kröhling, D., 1995. El Sistema Eólico Pampeano. In: Comunicaciones del Museo Provincial de Ciencias Naturales Florentino Ameghino (N.S.), vol. 5 (1), pp. 1–76.

Jain, M., Botter-Jensen, L., Singhvi, A.K., 2003. Dose evaluation using multiple-aliquot quartz OSL: test of methods and a new protocol for improved accuracy and precision. Radiat. Meas. 37, 67–80.

Jenny, B., Valero-Garces, B.L., Villa-Martinez, R., Urrutia, R., Geyh, M., Veit, H., 2002. Early to mid-Holocene aridity in central Chile and the southern Westerlies: the Laguna Aculeo record (34 degrees S). Quat. Res. 58 (2), 160–170.

Kemp, R.A., Toms, P.S., King, M., Kröhling, D.M., 2004. The pedosedimentary evolution and chronology of Tortugas, a Late Quaternary type-site of the northern Pampa, Argentina. Quat. Int. 114 (1), 101–112.

Kemp, R., Zárate, M.A., Toms, P., King, M., Sanabria, J., Arguello, G., 2006. Late Quaternary paleosols, stratigraphy and landscape evolution in the northern

Pampas, Argentina. Quat. Res. 66, 119–132.
Kocurek, G., Dott, R.H., 1981. Distinctions and uses of stratification types in the interpretation of eolian sand. J. Sediment. Petrol. 51 (2), 579–595.
Kocurek, G., Lancaster, N., 1999. Aeolian system sediment state: theory and Mojave Desert Kelso dune field example. Sedimentology 46 (3), 505–515.
Kröhling, D.M., 1999. Upper Quaternary geology of the lower Carcarañá Basin, north Pampa, Argentina. Quat. Int. 57–58, 135–148.
Kull, Ch, Grosjean, M., 2000. Late Pleistocene climate conditions in the north Chilean Andes drawn from a climate-glacier model. J. Glaciol. 46, 622–632.
Kuriyama, Y., Mochizuki, N., Nakashima, T., 2005. Influence of vegetation on aeolian sand transport rate from a backshore to a foredune at Hasaki, Japan. Sedimentology 52 (5), 1123–1132.
Lancaster, N., 1988. Development of linear dunes in the southwestern Kalahari southern Africa. J. Arid Environ. 14, 233–244.
Lea, P.D., 1990. Pleistocene periglacial eolian deposits in southwestern Alaska: sedimentary facies and depositional processes. J. Sediment. Petrol. 60, 582–591.
Leighton, C.L., Thomas, D.S.G., Bailey, R.M., 2014. Reproducibility and utility of dune luminescence chronologies. Earth Science Rev. 129, 24–39.
Machette, M., 1985. Calcic soils of southwestern United States. In: Weide, D.J. (Ed.), Soil and Quaternary Geology of the Southwestern United States. Geological Scociety of America, pp. 1–21. Special Paper 203.
Marengo, J.A., Soares, W., Saulo, C., Nicolini, M., 2004. Climatology of the low-level jet east of the Andes as derived from the NCEP–NCAR re-analyses: characteristics and temporal variability. J. Clim. 17, 2261–2280.
Markgraf, V., 1989. Palaeoclimates in central and south America since 18,000 BP based on pollen and lake-level records. Quat. Sci. Rev. 8, 1–24.
McKee, E.D. (Ed.), 1979. A Study of Global Sand Seas. U.S. Geological Survey. Professional Paper 1052, 429 pp.
Meier, H.A., Nordt, L.C., Forman, S.L., Driese, S.G., 2013. Late Quaternary alluvial history of the middle Owl Creek drainage basin in central Texas: a record of geomorphic response to environmental change. Quat. Int. 306, 24–41.
Mendes da Silva, G.A., Ambrizzi, T., 2010. Summertime moisture transport over Southeastern South America and extratropical cyclones behavior during inter-El Niño events. Theor. Appl. Climatol. 101, 303–310.
Miall, A.D., 1996. The Geology of Fluvial Deposits: Sedimentary Facies, Basin Analysis, and Petroleum Geology. Springer-Verlag, Berlin, p. 582.
Morrás, H.J.M., 1999. Geochemical differentiation of Quaternary sediments from the Pampean region based on soil phosphorus contents as detected in the early 20th century. Quat. Int. 62, 57–67.
Muhs, D.R., Holliday, V.T., 1995. Evidence of active dune sand on the great plains in the 19th century from accounts of early explorers. Quat. Res. 43 (2), 198–208.
Murray, A.S., Wintle, A.G., 2003. The single aliquot regenerative dose protocol: potential for improvements in reliability. Radiat. Meas. 37, 377–381.
Olley, J., Caitcheon, G., Murray, A., 1998. The distribution of apparent dose as determined by optically stimulated luminescence in small aliquots of fluvial quartz: implications for dating young sediments. Quat. Sci. Rev. 17, 1033–1040.
Piovano, E.L., Ariztegui, D., Córdoba, F., Cioccale, M., Sylvestre, F., 2009. Hydrological variability in South America below the tropic of capricorn (Pampas and eastern Patagonia, Argentina) during the last 13.0. In: Vimaux, Ka F., et al. (Eds.), Past Climate Variability in South America and Surrounding Regions, Developments in Paleoenvironmental Research, vol. 14, pp. 323–351.
Placzek, C., Quade, J., Betancourt, J.L., Patchett, P.J., Rech, J.A., Latorre, C., Matmon, A., Holmgren, C., English, N.B., 2009. Climate in the dry central Andes over geologic, millennial, and interannual timescales. Ann. Mo. Bot. Gard 96, 386–397.
Placzek, C.J., Quade, J., Patchett, P.J., 2006. Geochronology and stratigraphy of late Pleistocene lake cycles on the southern Bolivian Altiplano implications for causes of tropical climate change. Geol. Soc. Am. Bull. 118 (5–6), 515–532.
Placzek, C.J., Quade, J., Patchett, P.J., 2011. Isotopic tracers of paleohydrologic change in large lakes of the Bolivian Altiplano. Quat. Res. 75, 231–244.
Prescott, J.R., Hutton, J.T., 1994. Cosmic ray contributions to dose rates for luminescence and ESR dating: large depths and long-term time variations. Radiat. Meas. 23, 497–500.
Prieto, M.R., Rojas, F., 2012. Climatic variations in the Cordillera de Los Andes and their consequences over the environmental and social processes in the Mendoza Northern Oasis, between the 19th and 20th Century. Clim. Past 8, 951–961.
Prieto, M.R., Abraham, E., Dussel, P., 2008. Transformaciones de un ecosistema palustre. La gran ciénaga del Bermejo- Mendoza, siglos XVIII y XIX. Multequina 17, 147–164 (IADIZA).
Pye, K., Tsoar, H., 2009. Aeolian Sand and Sand Dunes, second ed. Springer, Berlin, p. 476.
Reading, H.G., 1996. Sedimentary Environments: Processes, Facies and Stratigraphy, third ed. Blackwell Science, p. 704.
Rhodes, R.H., Faïn, X., Stowasser, C., Blunier, T., Chappellaz, J., McConnell, J.R., Romanini, D., Mitchell, L.E., Brook, E.B., 2013. Continuous methane measurements from a late Holocene greenland ice core: atmospheric and in-situ signals. Earth Planet. Sci. Lett. 368, 9–19.
Roberts, H.M., 2012. Testing post-IR IRSL protocols for minimising fading in feldspars, using Alaskan loess with independent chronological control. Radiat. Meas. 47 (9), 716–724.
Roberts, R.G., Galbraith, R.F., Olley, J.M., Yoshida, H., Laslett, G.M., 1999. Optical dating of single and multiple grains of quartz from Jinmium rock shelter, northern Australia. Part II, results and implications. Archaeometry 41, 365–395.
Rojo, L., Mehl, A.E., Páez, M.M., Zárate, M.A., 2012. Mid- to Late Holocene pollen and alluvial record of the arid Andean piedmont between 33° and 34°S, Mendoza, Argentina: inferences about floodplain evolution. J. Arid Environ. 77, 110–122.
Ruegg, G.H.J., 1983. Periglacial evenly laminated sandy deposits in the late Pleistocene of N.W.Europe, a facies unrecorded in modern sedimentological handbooks. In: Brookfield, M.E., Ahlbrandt, T.S. (Eds.), Eolian Sediments and Processes. Elsevier, Amsterdam, pp. 455–482.
Rutter, N., Coronato, A., Helmens, K., Rabassa, J., Zárate, M., 2012. Glaciations in North and South America from the Miocene to the Last Glacial Maximum: Comparisons, Linkages and Uncertainties. Springer Briefs in Earth System Sciences, p. 67.
Salio, P., Nicolini, M., Saulo, C., 2002. Chaco low-level jet events characterization during the austral summer season. J. Geophys. Res. Atmos. 107, 4816.
Sandweiss, D.H., Maasch, K.A., Anderson, D.G., 1999. Transitions in the Mid-Holocene. Science 83 (5401), 499–500.
Servicio Meteorológico Nacional (SMN). Estadísticas Climatológicas 1981-1990, 1991-2000. Buenos Aires. Argentina.
Singhvi, A.K., Porat, N., 2008. Impact of luminescence dating on geomorphological and palaeoclimate research in drylands. Boreas 37 (4), 536–558.
Silva, V.B.S., Kousky, V.E., 2012. The South American monsoon system: climatology and variability. In: Wang, S., Gillies, R.R. (Eds.), Modern Climatology. InTech, p. 398.
Smith, J.A., Rodbell, D.T., 2010. Cross-cutting moraines reveal evidence for North Atlantic influence on glaciers in the tropical Andes. J. Quat. Sci. 25, 243–248.
Spooner, N.A., 1994. The anomalous fading of infra-red stimulated luminescence from feldspars. Radiat. Meas. 23, 625–632.
Sylvestre, F., 2009. Moisture pattern during the Last glacial maximum in South America. In: Vimaux, K.F., et al. (Eds.), Past Climate Variability in South America and Surrounding Regions, Developments in Paleoenvironmental Research, vol. 14, pp. 3–27.
Sylvestre, F., Servant, M., Servant-Vildary, S., Causse, C., Fournier, M., Ybert, J.P., 1999. Lake level chronology on the southern Bolivian Altiplano (18°-23°S) during Late-glacial time and the Early Holocene. Quat. Res. 51, 54–66.
Tchilinguirian, P., Morales, M.R., 2013. Mid-Holocene paleoenvironments in northwestern Argentina: main patterns and discrepancies. Quat. Int. 307, 14–23.
Trauth, M.H., Strecker, M.R., 1999. Formation of landslide-dammed lakes during a wet period between 40,000 and 25,000 years BP in northwestern Argentina. Palaeogeogr. Palaeoclimatol. Palaeoecol. 153, 277–287.
Tripaldi, A., Forman, S.L., 2007. Geomorphology and chronology of Late Quaternary dune fields of western Argentina. Palaeogeogr. Palaeoclimatol. Palaeoecol. 251 (2), 300–320.
Tripaldi, A., Zárate, M.A., 2014. A review of Late Quaternary inland dune systems of South America east of the Andes. Quat. Int. http://dx.doi.org/10.1016/j.quaint.2014.06.069.
Tripaldi, A., Ciccioli, P.L., Alonso, M.S., Forman, S.L., 2010. Petrography and geochemistry of late Quaternary dune fields of western Argentina: provenance of aeolian materials in southern South America. Aeolian Res. 2 (1), 33–48.
Tripaldi, A., Zárate, M.A., Brook, G.A., Li, G.Q., 2011. Late Quaternary paleoenvironments and paleoclimatic conditions in the distal Andean piedmont, southern Mendoza, Argentina. Quat. Res. 76 (2), 253–263.
Tripaldi, A., Zárate, M.A., Forman, S.L., Badger, T., Doyle, M., Ciccioli, P.L., 2013. Geological evidence for a drought episode in the western Pampas (Argentina, South America) during the early–mid 20th century. Holocene 23 (12), 1729–1744.
Vilanova, I., Schittek, K., Geilenkirchen, M., Schabitz, F., Schulz, W., 2015. Last millennial environmental reconstruction based on a multi-proxy record from Laguna Nassau, Western Pampas, Argentina. Neues Jahrb. Geol. Paläontol. 277, 209–224.
Villagrán, C., Varela, J., 1990. Palynological evidence for increased aridity on the Central Chilean during the Holocene. Quat. Res. 34, 198–207.
Wang, M., Paegle, J., 1996. Impact of analysis uncertainty upon regional atmospheric moisture flux. J. Geophys. Res. 101 (D3), 7291–7303.
Wright, D., Forman, S.L., Waters, M., Ravesloot, J., 2011. Holocene eolian activity as a proxy for broad-scale landscape change on the Gila River Indian community, Arizona. Quat. Res. 76 (1), 10–21.
Wintle, A.G., Murray, A.S., 2006. A review of quartz optically stimulated luminescence characteristics and their relevance in single-aliquot regeneration dating protocols. Radiat. Meas. 41, 369–391.
Woodward, C., Shulmeister, J., Larsen, J., Jacobsen, G.E., Zawadzki, A., 2014. The hydrological legacy of deforestation on global wetlands. Science 346, 844–847.
Zárate, M.A., 2003. Loess of southern South America. Quat. Sci. Rev. 22, 1987–2006.
Zárate, M.A., 2007. South American loess record. In: Elias, S.A. (Ed.), The Encyclopedia of Quaternary Science, vol. 2. Elsevier, Amsterdam, pp. 1466–1479.
Zárate, M.A., Tripaldi, A., 2012. The aeolian system of central Argentina. J. Aeolian Res. 3, 401–417.
Zárate, M., Kemp, R.A., Espinosa, M., Ferrero, L., 2000. Pedosedimentary and palaeoenvironmental significance of a Holocene alluvial sequence in the southern Pampas Argentina. Holocene 10 (4), 481–488.
Zárate, M., Kemp, R., Toms, P., 2009. Late Quaternary landscape reconstruction and geochronology in the northern Pampas of Buenos Aires province, Argentina. J. S. Am. Earth Sci. 27, 88–99.
Zech, W., Zech, M., Zech, R., Peinemann, N., Morrás, H., Moretti, L., Ogle, N., Kalim, R., Fuchs, M., Schad, P., Glaser, B., 2009. Late Quaternary palaeosol records from subtropical (38° S) to tropical (16° S) South America and palaeoclimatic implications. Quat. Int. 196, 107–120.